

## Response Corridors of Human Surrogates in Lateral Impacts

**Matthew R. Maltese, Rolf H. Eppinger, Heather Rhule, Bruce Donnelly**

National Highway Traffic Safety Administration

**Frank A. Pintar and Narayan Yoganandan**

Medical College of Wisconsin and Veterans Affairs Medical Center – Milwaukee

---

**ABSTRACT** – Thirty-six lateral PMHS sled tests were performed at 6.7 or 8.9 m/s, under rigid or padded loading conditions and with a variety of impact surface geometries. Forces between the simulated vehicle environment and the thorax, abdomen, and pelvis, as well as torso deflections and various accelerations were measured and scaled to the average male. Mean  $\pm$  one standard deviation corridors were calculated. PMHS response corridors for force, torso deflection and acceleration were developed. The offset test condition, when partnered with the flat wall condition, forms the basis of a robust battery of tests that can be used to evaluate how an ATD interacts with its environment, and how body regions within the ATD interact with each other.

**KEYWORDS** – side impact, biofidelity, sled test, corridor, dummy

---

### INTRODUCTION

The development of side impact safety systems in motor vehicles requires an anthropomorphic test device (ATD) that performs similar to a would-be human occupant in the same crash condition. Such an ATD must load the vehicle interior in a manner similar to the human and provide sufficient information to estimate injury. Thus, it is necessary to develop test procedures and performance requirements to ensure that an ATD is human-like in its intended mode of use.

Several researchers have developed test procedures and associated corridors and boundaries wherein the ATD responses should lie (ISO/TR9790 1997, Roberts et al. 1990, Eppinger 2001). Developing such response requirements and test procedures generally entails exposing a biological model (human cadaver, primate) of the living human to an impact similar to a vehicle crash. Experiments that form the basis of ATD response requirements are generally performed in an environment that simulates the full vehicle test. Morgan et al. (1981 and 1986) conducted a series of flat impact surface side impact PMHS (post-mortem human subject) and dummy sled tests under padded and rigid impact conditions at 6.7 and 8.9 m/s. Cavanaugh et al. (1993) conducted side impact sled tests under padded and rigid flat-impact surface conditions and

presented normalized impact surface force, occupant acceleration, and torso deflections.

Cavanaugh et al. (1996) supplemented this work by investigating the role of impact surface geometry in injury prediction and proposed an armrest stiffness limit. Based upon the same test series, Zhu et al. (1993) characterized the mechanical response of the pelvis, and Irwin et al. (1993) analyzed the shoulder response. Rouhana and Kroell (1989) conducted a series of side impact sled tests with anesthetized swine and found that load-surface discontinuities can cause significant injury, thus emphasizing the importance of impact surface geometry in vehicle design. Viano (1989) conducted oblique thorax and abdomen pendulum impacts, and lateral pelvis impacts to PMHS and developed force vs. time and force vs. deflection corridors for each body region.

Impact testing yields a vast amount of kinetic and kinematic data from each experiment. Variations in specimen size and material properties lead to variations in the same measured response from specimen-to-specimen despite identical test conditions. Scaling procedures have been developed in an attempt to account for biological variability. Eppinger (1976) developed force, acceleration, deflection and time scale factors as a function of PMHS density, modulus, and mass. Mertz (1984) developed a procedure for determining scale factors

by modeling the subject response with a single mass-spring system. Krause (1984) proposed a regression technique for normalization of biomechanical responses.

After specimen measurements have been scaled, it is necessary to quantify the response of the test series to develop the average response. Two techniques have been developed to quantify and summarize measurements from several scaled test specimens. Lobdell et al. (1973) created corridors by drawing an "eyeball average" through the data and then creating points at  $\pm 15\%$  of the average. Cavanaugh et al. (1986) and Morgan et al. (1986) employed a corridor calculation technique of determining mean and standard deviation of a group of signals at each point in time. The corridor was developed by adding/subtracting the standard deviation at each time point along the mean response (Figure 1).

**METHODS**

For this effort, 36 side impact PMHS sled tests were conducted at the Medical College of Wisconsin (MCW) and the NHTSA Vehicle Research and Test Center (VRTC) in cooperation with the Ohio State University (Pintar et al. 1997)<sup>1</sup>. Tests were conducted at a variety of speeds, with and without impact surface padding, and using a variety of impact wall geometries (Appendix B).

**Subject Preparation**

Both unembalmed fresh and fresh frozen cadaver

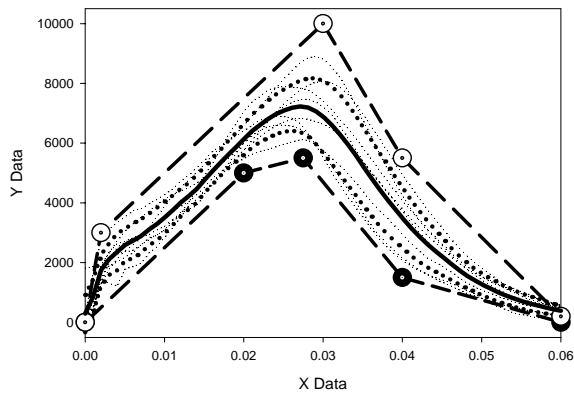


**Figure 1.** Example of two different corridor construction techniques – solid line is the moving average with standard deviation shown in a dotted line; long dashed line is the "eyeball" method.

<sup>1</sup>All testing was reviewed and approved by NHTSA's Human Use Review Panel (HURP) and the Institutional Review Boards of either the Medical College of Wisconsin or Ohio State University.

subjects were used as experimental subjects. Radiographic examination of all body regions and medical records were examined to exclude specimens with bone disease and metastatic cancer; deaths were primarily attributed to cardiopulmonary disease. Subjects were cleaned and dressed in a tight-fitting leotard and head/face mask to ensure confidentiality. Instrumentation of test subjects included either two or three chestbands (Eppinger 1978). The upper thorax chestband was placed just below the axilla, the lower thorax band at the base of the sternum, and the abdominal band, when present, at the mid-abdomen level. Tri-axial accelerometers were attached to the upper spine (spinous process of the T1, T2, T3, or T4 vertebra), to the lower spine (spinous process of T12), and to the pelvis (posterior aspect of the sacrum). The tri-axial accelerometers were oriented such that positive z-acceleration was down, y-acceleration was positive to the right, and x-acceleration was positive in the posterior-to-anterior direction. The lateral aspects of the left and right upper rib (rib 4) and left and right lower rib (rib 8), were instrumented with uni-axial accelerometers with the sensitive axis left-right. The vascular system of the MCW test subjects was pressurized; the VRTC subjects were not pressurized.

**Sled Apparatus**

The sled apparatus was of the Heidelberg (Kallieris et al. 1981) design and was propelled on a rebound sled at MCW and a HyGe acceleration track at VRTC. Test subjects were seated on the bench of the side impact sled approximately one meter from the load wall. Change in velocity was achieved by deceleration and rebounding (rebound sled) or rapid acceleration (HyGe sled). This caused the unrestrained test subject to slide relative to the sled toward the load wall. Just after the sled achieved the

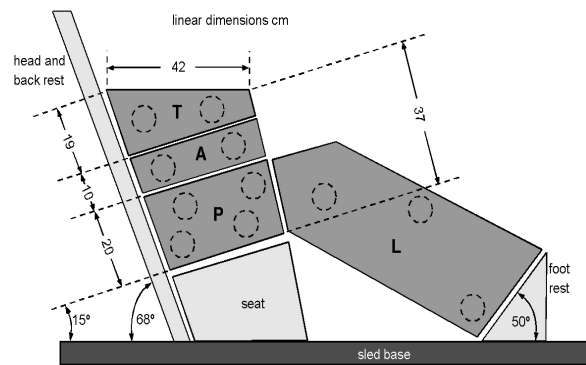


**Figure 2.** MCW/VRTC side impact buck showing load plates for the thorax (T), abdomen (A), pelvis (P) and leg (L).

prescribed velocity change, the occupant contacted the load wall. The sled continued to move along the track at near-constant velocity during occupant-to-load wall interaction. The sled was then gradually slowed by a braking system.

The load wall was divided into four sections, one each to contact the thorax, abdomen, pelvis and legs (Figure 2). Force transducers between the sled and load plates measured occupant loads from each body region. The change in sled velocity was either 6.7 or 8.9 ( $\pm 0.3$ ) m/s. The load wall was either rigid or padded with 10 cm of LC200 padding (compressive stiffness = 103 kPa). The geometry of the load wall was also a variable. Load plates were either fixed in the same plane, or the thoracic, abdominal or pelvic plate was offset, one at a time per test, toward the occupant by 11 cm. In flat wall and pelvic offset tests, the PMHS was seated with arms down and hands on lap, such that the arm was interposed between the thorax and load wall. In thoracic and abdominal offset tests, arms were raised to expose the thorax and abdomen directly to impact from the load wall.

High-speed 16-mm film and digital video cameras recorded the side impact event. There was one overhead view, one onboard anterior view and two offboard posterior views.

**Corridor Development**

Tests were grouped by initial condition: rigid high-speed flat wall (RHF), padded high-speed flat wall (PHF), rigid low-speed flat wall (RLF), padded low-speed flat wall (PLF), rigid low-speed thoracic offset (RLT), rigid low-speed abdominal offset (RLA), rigid low-speed pelvic offset (RLP) and padded low-speed pelvic offset (PLP). For each group of tests with the same initial conditions, signals with the same instrumentation type and locations (e.g., upper spine acceleration, upper thorax deflection) were grouped together into *signal groups*.

*Signal Processing*

All acceleration and force signals were filtered according to SAE J211, and subsampled at 3200 Hz. Chestband gauge signals were filtered at CFC 600, and torso deformation contours were calculated at 0.001-second intervals. The following process was used to determine full chest deflection:

1. Six locations on each deformation contour were selected for development of full torso deflections (Figure 3a). Starting at the spine

and following the contour in a clockwise direction, locations were marked at 20%, 25%, 30%, 70%, 75%, and 80% of the contour's circumference.

2. The straight-line distance between location pairs 30% and 70%, 25% and 75%, and 20% and 80% were calculated and averaged to provide mean torso deflection.
3. Steps 1 and 2 were repeated for subsequent time steps to create individual and averaged full deflection time histories for a particular chestband.

The left half-chest deflection was determined as follows:

1. A mid-sagittal line was constructed between the sternum (the point 50% along the band circumference) and spine (the point 0% along the band circumference) locations on the chestband (Figure 3b).
2. The perpendicular distance between the previously determined 20%, 25%, and 30% points and the mid-sagittal line was averaged to determine the half-thoracic deflection.
3. Steps 1 and 2 were repeated for each subsequent time step to create the left half deflection time history for a particular chestband. Sternum and spine locations were considered to remain at 50% and 0% along the contour circumference respectively, throughout the event.

*Scaling Process*

Mass scaling (Eppinger et al. 1984) was employed to normalize the data to a 50<sup>th</sup> percentile male subject. Assuming the moduli of elasticity and density are

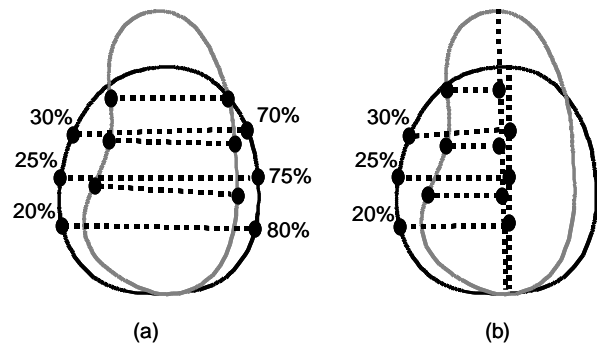


**Figure 3.** Techniques for calculating full (a) and half (b) thorax and abdomen deflections from chestband contour data.

equal between subjects, mass-based scaling was used on all force, deflection and acceleration signals according to:

$$\begin{aligned}
 \text{Velocity: } & V_s = V_i \\
 \text{Acceleration: } & A_x = \lambda_m^{-1/3} A_i \\
 \text{Deflection: } & D_s = \lambda_m^{1/3} D_i \\
 \text{Time: } & T_s = \lambda_m^{1/3} T_i \\
 \text{Force: } & F_s = \lambda_m^{2/3} F_i
 \end{aligned}
 \tag{Equation 1}$$

where s is the subscript for scaled data, i is the subscript for i-th test subject and:

$$\lambda_{m_i} = \frac{75}{m_i}
 \tag{Equation 2}$$

where m is the subject mass in kilograms.

#### Signal Timing Issues

It was required for each test to have a uniform reference for time, or time-zero, for all signals recorded during the test. For flat wall tests, time-zero was determined by initiation of arm contact on the thoracic load plate. In pelvic, thoracic and abdominal offset tests, time-zero was coincident with specimen contact with the offset load plate. Contact with the load plate was determined by finding the first point in time on the load wall force-time history where the load exceeded 200 N and then incrementing backward to find the point in time where the force-time history crossed zero load (zero-crossing load). The time of occurrence of the zero-crossing load was taken to be the start of the impact event for all recorded signals.

After overlaying the signals in each signal group, it became apparent that while signals seemed to have the same shape, the time of occurrence of the signals varied from test subject to test subject despite mass scaling. For example, the amount of time for pelvis acceleration to achieve maximum value post-time-zero was different from test subject to test subject, yet the shape and magnitude of the signal seemed essentially the same. This variability was primarily attributed to differences in the ratio of thoracic breadth to pelvic breadth, thoracic breadth to abdominal breadth, or slight variations in the posture of the test subject as it contacted the impact surface.

One solution considered was to determine a separate time-zero for each body region, similar to procedures followed by the International Standards Organization (ISO). In such a scheme, the thorax load plate contact time would establish time-zero for the thorax load wall force and all associated kinematic instrumentation (T1 acceleration, thorax deflection), the abdominal load plate contact time would establish time-zero for the abdomen load plate force and the abdominal deflection, and the pelvis load plate would establish time-zero for the pelvis load wall force and the pelvis acceleration. With this scheme, the relative timing information between body regions is lost, and it becomes somewhat challenging to establish time-zero for sensors located at the interface between body regions, such as the T12 accelerometer that could be associated with either the thorax or abdomen. This technique was applied by the ISO committee to evaluate flat wall sled tests.

In the present study, a portion of the tests were conducted in the offset condition. This condition was specifically designed to evaluate the interface between body regions, thus providing important information about response of the thorax when the pelvis is struck first. Accordingly, a requirement was implemented to preserve relative timing information between sensors attached to different body regions. Therefore, an analysis scheme was developed by which the shape and magnitude of each signal were represented in the form of a corridor, and the time of occurrence of each signal was quantified.

#### Characteristic Time

In order to quantify when a particular signal occurred relative to time-zero, a *characteristic time* for each signal was defined as follows (Figure 4). For force and deflection signals, the maximum value of the signal time-history was determined. Starting from the maximum value, the signal trace was followed backward in time until the magnitude was reduced to 20% of the maximum value. The characteristic time of a particular signal was defined as the time of occurrence, relative to time-zero, of the 20%-of-maximum value. The characteristic time for acceleration signals was determined in the same manner, except that the acceleration signal was first integrated and then the maximum and 20%-point of the integrated acceleration were determined. After determining characteristic time, the integrated acceleration curve was discarded and the characteristic time was associated with the original acceleration curve. *Average characteristic time* for each signal group was determined to quantify the

average time at which the signals in the group occurred relative to experimental time-zero.

$$V_{ab} = \sum_t^{t'} (a_i - b_i)^2 \quad \text{Equation 3}$$

*Signal Alignment*

After the *characteristic time* of each signal in the signal groups was established, a process was developed to quantify the shape and magnitude of each signal group. As mentioned previously, the shape and magnitude of signals from certain instruments were relatively invariant from test to test; however, at times the signals were significantly out of phase. To develop a reasonable average shape and magnitude, one could envision “pushing” the signals forward and backward in time until they overlaid one another. An automatic process for doing so was developed, and the signals in each signal group were aligned according to the following minimization of cumulative variance technique.

The cumulative variance between signals a and b ( $V_{ab}$ ) was determined from the following equation,

where

$a_i$  is the magnitude of signal a at the  $i^{\text{th}}$  time step

$b_i$  is the magnitude of signal b at the  $i^{\text{th}}$  time step

$t$  is the greater of the start time (defined below) of signal a and the start time of signal b

$t'$  is the lesser of the end time (defined below) of signal a and end time of signal b

Signal start and end time were not simply the length of the recording time. Depending upon the amount of pre- and post-impact data collected, the signal alignment algorithm was focused on uninteresting portions of the signal collected significantly before or after the primary impact event. To avoid this case, the duration of interest was defined as follows:

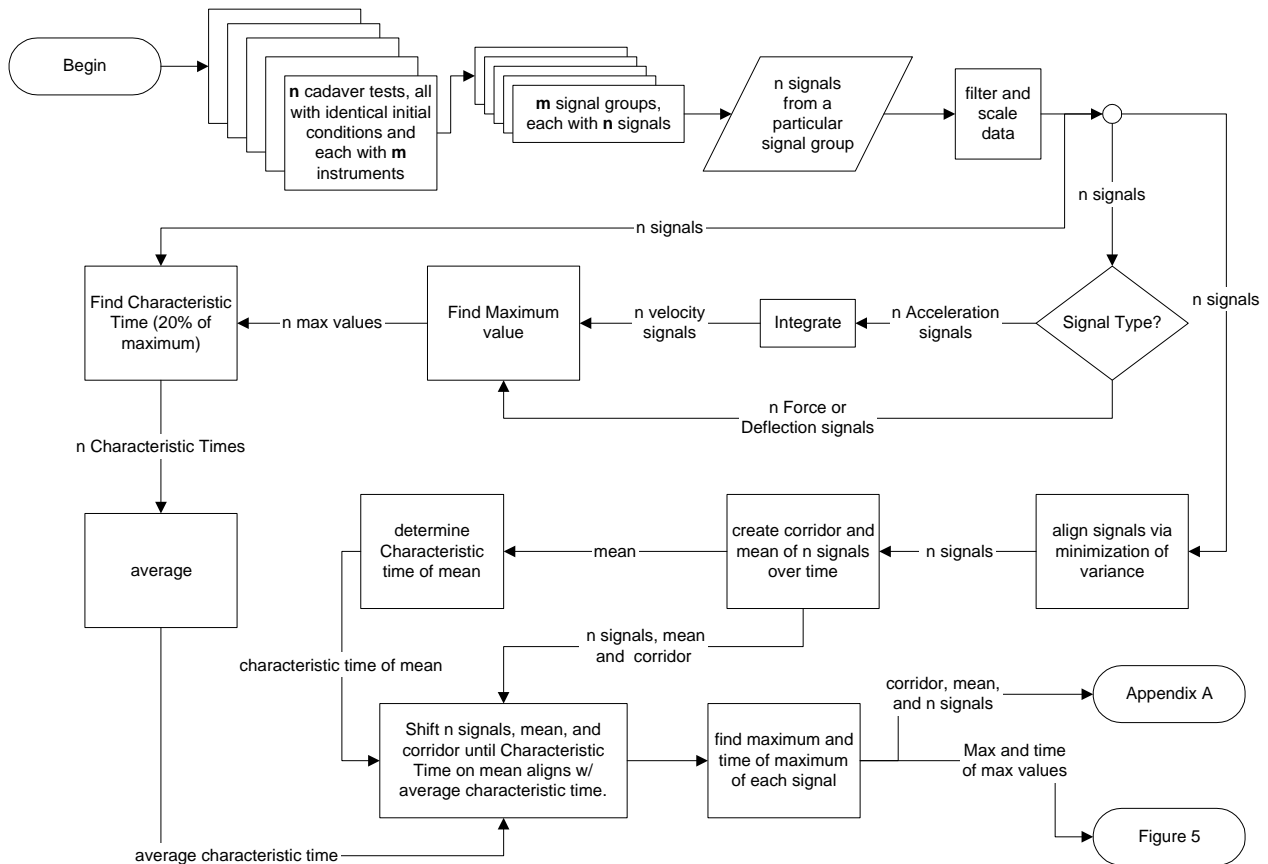


Figure 4. – Flow chart of process for calculating corridors from test data.

1. For force and deflection signals, starting from the maximum of the signal, increment backward in time until the signal magnitude reached 20% of the maximum value. Record this time as the *start time* of the signal. Again starting from the maximum of the signal, increment forward in time until the signal magnitude reached 20% of the maximum value. Record this time as the *end time* of the signal.
2. For acceleration signals, the curve is first integrated, and then the maximum value is determined. Beginning at the maximum value and incrementing backward, the end time is the time of the first point that reaches 80% of the maximum value, and the start time is the time of the first point that reaches 20% of the maximum value.

Two signals can be aligned by time-shifting the signals relative to one another until a minimum variance (Equation. 3) would be obtained. However, in the present study, it was desired to align a set of n signals. To do so, one signal from each signal group was chosen as the alignment standard. This alignment standard was the one that appeared to have the most typical shape of all signals. The cumulative variance between the alignment standard signal (S) and the second signal (2) in the group,  $V_{S2}$ , was minimized as follows. The second signal was shifted backward in time by an amount equal to one-third of its duration (end time minus start time), and the variance  $V_{S2}$  calculated according to Equation 1. The second signal was then shifted forward in time by one time step, and the cumulative variance calculated and stored. The process of shifting and calculating the variance continued until the second signal had been forward time-shifted by an amount equal to two-thirds of its total duration; the variance was recorded at each shift step. The shift step with the lowest cumulative variance was considered to have the optimal alignment of the alignment standard and second signals. The process was repeated for all signals in the group, optimally aligning them with the standard signal, one at a time.

*Corridor Calculation*

The mean response at each time t (after alignment) across n signals in a group was calculated by:

$$\bar{x}_t = \sum_{i=1}^n \frac{x_{i,t}}{n} \tag{Equation 4}$$

where:

n is the number of signals

x is the magnitude of the signal

Standard deviation (SD) at each time t was then calculated as:

$$SD_t = \left[ \sum_{i=1}^n \frac{(x_{i,t} - \bar{x}_t)^2}{n-1} \right]^{1/2} \tag{Equation 5}$$

and the upper and lower corridors were determined by:

$$\begin{aligned} \text{Upper Corridor : } U_t &= SD_t + \bar{x}_t \\ \text{Lower Corridor : } L_t &= SD_t - \bar{x}_t \end{aligned} \tag{Equation 6}$$

Standard deviation corridors were calculated for signal groups where at least three signals were available. In conditions where only two time-histories were available, the upper and lower corridors were determined by multiplying the PMHS mean response-time curve by 1.2 and 0.8 respectively.

The alignment process (Equation 3) shifted all signals in a particular signal group until optimally aligned with the standard signal. The position of the standard signal in time was dependent upon the characteristics of the test subject on which it was measured, and was not necessarily representative of all the subjects in the signal group. Thus, the position of the corridor in time was somewhat arbitrary at that point in the analysis. To compensate, the characteristic time of the mean of the corridor was determined. The mean corridor and signal group were shifted in time until the characteristic time of the corridor was equal to the average characteristic time for the signal group. The maximum and time of maximum of each of the signals in a signal group was also determined. The mean and standard deviation of the maximum values were determined as well as time of maximum values.

**RESULTS**

The processed signals from each test and the associated corridors for force, acceleration, and thorax and abdomen deflection are given in Appendix A and can be downloaded from the NHTSA Web page<sup>2</sup>. The mean ± the standard deviation of the

<sup>2</sup><http://www-nrd.nhtsa.dot.gov/departments/nrd-51/BiomechanicsTrauma.html>

maximum values of each signal in a signal group and the associated mean  $\pm$  the standard deviation of the time of maximums are also plotted (Figure 5).

The reduction in speed between rigid high-speed flat wall and rigid low-speed flat wall test conditions reduced magnitude and increased time-to-peak of thoracic forces (Figure 5a). A similar trend existed in the abdominal and pelvis data, however the trend was not as clear (Figures 5b and c). The addition of padding also reduced the magnitude and time to peak of forces in the flat wall tests (Figures 5a, b and c). In general, abdominal corridors were half-sine shaped in the case of the padded flat wall tests and bimodal in unpadded flat wall tests (Appendix A2).

The addition of padding to the low-speed pelvis offset test also reduced the magnitude and increased the time-to-peak of pelvis force (Figure 5c). Abdominal forces were highest in the abdominal offset condition (Figure 5b). Despite the offset, the RLT condition did not generate the highest thoracic loads, as increased speed in the rigid high-speed flat wall condition led to higher but slightly later occurring thoracic loads than the rigid low-speed thoracic offset condition. Similarly, pelvis loads were higher in the rigid high-speed flat wall condition than in the rigid low-speed pelvis offset condition. Variability in the impact time was highest in RLF test condition.

The addition of padding to the flat wall high- or low-speed test conditions reduced peaks and increased time-to-peak of the T1 accelerations. A similar trend was observed for the reduction in test speed (Figure 5d). The lower spine acceleration behaved similarly; however, padding in the low-speed flat wall condition only delayed time-to-peak with little or no influence on magnitude (Figure 5e). Pelvic acceleration in the flat wall condition showed a similar trend as the upper spine acceleration; time-to-peak was increased and magnitudes were decreased with the introduction of padding or reduction in test speed. However, in the RLF condition the time-to-peak demonstrated additional variability.

The addition of offset to the flat wall condition, regardless of offset location, had little effect on the maximums of upper and lower spine acceleration, but increased the elapsed time to achieve such maximums. Spine accelerations took the longest time to reach maximum in the pelvis offset tests, followed by abdominal tests, and then thoracic

offset tests (Figures 5d and e). No clear trend was observed in pelvic acceleration (Figure 5f).

The magnitude of upper and lower thorax deflections in flat wall tests was not significantly influenced by the change in test conditions. Time of maximum upper thorax deflection was dependent upon test condition and peaked earliest in the rigid high-speed condition, followed by the padded high-speed, rigid low-speed, and padded low-speed, all for flat wall tests (Figure 5g). Similar trends were observed in the lower thoracic deflection; however, discrimination between time of peak was not as pronounced since the rigid low-speed and padded high-speed test results overlap in time (Figure 5h). Abdominal deflections in the high-speed condition were greater than those in the low-speed condition. In all cases, the pelvis offset condition led to the greatest time-to-peak in any of the deflections, and the abdominal offset condition had the largest deflection of the low-speed test (Figures 5g, h and i). Half-thorax deflections were 55% to 66% of full-thorax deflections in the flat wall condition (Table 1 and Appendix A9-A14).

## **DISCUSSION**

Through the use of an impact surface with variable geometry, the tests presented not only measure response of individual body regions, but examine the interface between several key body regions and offer data to evaluate ATDs in similar interface conditions. For example, pelvic offset condition reduced the magnitude of the thorax load plate force when compared with flat wall tests at the same speed and padding. Thus, designing a restraint system that strikes the pelvis before the thorax should reduce thoracic load. However, it is important that the lumbar region of ATDs accurately transmit the load from pelvis to thorax to ensure the appropriate reduction in thoracic load is human-like. Thoracic, abdominal or pelvis offset all result in considerably different PMHS load wall responses (Figure 5). In each case, the load wall with the offset carries the greatest load and often shields its neighboring load plates from experiencing any load. Half-thorax deflections were significantly less than full-thorax deflections, indicating substantial motion of the non-struck side of the thorax during the impact. As with any kinematic measure, deciding whether an ATD should reproduce either full- or half-thorax deflection should be based upon the capability of those measures to predict injury.

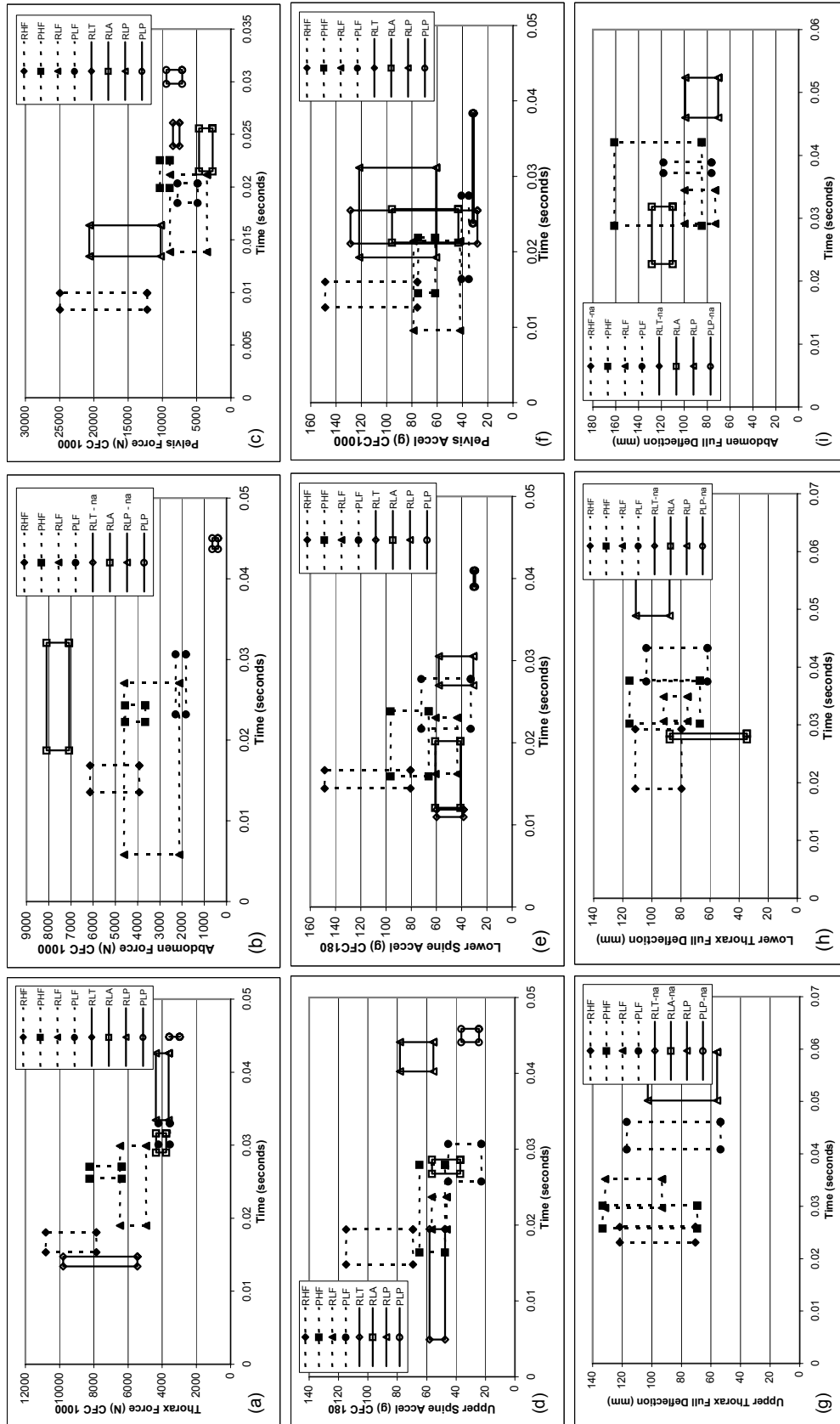


**Figure 5.** Mean  $\pm$  one standard deviation of the maximum values for each signal in a signal group vs. time of the maximum values for each signal in a signal group, plotted for different test conditions. Legend test conditions are defined as follows: RHFF=rigid high-speed flat wall, PHFF=padded high-speed flat wall, RLF=rigid low-speed flat wall, PHF=padded low-speed flat wall, RLT=rigid low-speed thoracic offset, RLA=rigid low-speed abdominal offset, RLP=rigid low-speed pelvic offset, and PLP=padded low-speed pelvic offset.

**Table 1.** Maximum of the mean deflection time history for the full and half-upper thorax, lower thorax and abdomen

Test Condition		Deflection (mm)			
		RHF	PHF	RLF	PLF
Measurement Location					
Upper thorax	Full	95	89	110	85
	Half	58	60	72	56
	% Half/Full	61.1%	67.4%	65.5%	65.9%
Lower thorax	Full	93	100	82	82
	Half	58	55	51	52
	% Half/Full	62.4%	55.0%	62.2%	63.4%
Abdomen	Full	n/a	118	86	98
	Half	n/a	78	52	58
	% Half/Full	n/a	66.1%	60.5%	59.2%

The addition of padding or reduction in test speed reduced the magnitude of peak wall forces and also increased the time to achieve such forces. Abdominal forces in high- and low-speed rigid flat wall tests were bi-modal. Film data demonstrated the arm first striking the load wall and then rebounding slightly. The body then followed to fully engage the load wall plate. The presence of padding, however, attenuated the initial arm contact such that the abdominal force trace was more uni-modal.

The RLF had a higher degree of variability than the other test conditions; however, no justification could be formed to eliminate any of the tests based upon pre-impact conditions or PMHS characteristics. Therefore, it was presumed that all tests in the RLF condition were as representative of the driving population as any of the other test conditions. Thus, all tests in the RLF condition were included in the analysis.

Our measurement of half-deflection (Figure 4) is not the same measurement as that used by other authors. For example, Viano (1989) measured deflection of the struck side with respect to the spine using a camera system. Targets affixed to the spine served as a reference point, although these tests were also conducted at 30 degrees forward of a lateral angle. Irwin (1993) also measured thoracic deflection in sled tests by determining relative displacement of the spine with respect to the impacting load wall using film analysis. Our left side half-deflection is not affixed to the spine only, but is also affixed to a line between the sternum and spine. Presuming the sternum would undergo lateral displacement with respect to the spine during impact, the half-thorax/abdomen deflections reported in this work may differ from those of other authors.

The magnitude of the upper and lower thorax deflections in the flat wall tests was not significantly influenced by the change in test conditions, although time of peak was influenced. Since data were scaled to the 50<sup>th</sup> percentile male, the expectation was that the maximum of the average deflection for RHF would be greater than RLF, and a similar trend would exist between PHF and PLF, RHF and PHF, and RLF and PLF. It is possible the rib structure in the thorax does not behave in a linear manner in these tests at these intensities; the rib structure may simply collapse. It is important to note that abdominal deflections increased with test severity, further supporting the hypothesis that ribs collapse at these intensities.

**Comparison with ISO TR 9790**

Corridors from the ISO (ISO/TR9790 1997) were compared with corridors presented in this study. The ISO specifications consist of absolute maximum value ranges for a particular signal or corridors developed by drawing a series of straight lines around the data.

The ISO specifications dictate use of Wayne State University (WSU) and Heidelberg sled systems, which differ in geometry from the NHTSA sled. Specifically, the top edge of the load surface on the NHTSA sled does not engage the shoulder like the Heidelberg and WSU sleds (Figure 6). The WSU and NHTSA load walls offer similar abdominal load plates, while the Heidelberg sled has no load plate in the abdominal region. Pelvis load plates of the Heidelberg and NHTSA sleds engage both the greater trochanter and iliac wing; however, the WSU sled only engages the greater trochanter.

The ISO rib acceleration absolute maximum corridor overlapped with the RLF corridor, but ISO upper and

lower spine accelerations were higher than the RLF corridor (Figure 7). The ISO pelvis acceleration corridors overlapped with the higher end of the RLF and RHF corridors. The ISO specifies two padded high-speed acceleration corridors, each with

23 psi and 15 psi crushable paper honeycomb padding. The ISO pelvis acceleration corridors for the 23 psi padded high-speed environment overlapped with the corresponding corridor from the present study, and the 15 psi ISO pelvis tests were higher than the corridor from the current investigation.

The magnitude of ISO thoracic and abdominal force corridors was similar to those presented in the current study (Figure 8). The ISO pelvis force vs. time corridors were similar to the corresponding RLF corridors. The ISO specifies two pelvis force corridors from the RHF condition, one filtered at CFC 1000 and the other filtered at FIR100. Compared to the work presented here, the CFC 1000-filtered data show the ISO corridors are lower, while the FIR 100-filtered data demonstrate the ISO corridors are higher.

Despite the difference in load wall geometry and absence of a shoulder plate in the current study, thorax and abdominal forces were similar to those found in ISO. The ISO analysis combined shoulder and thorax load cells and published them in the specifications.

**CONCLUSIONS**

Using the techniques discussed in this paper, the responses of multiple PMHS experiencing identical initial impact conditions have been characterized by average time histories and accompanied by  $\pm$  standard deviation time histories that characterize confidence bands for these responses. Additionally, phasing between signals from a particular signal group has been preserved. By applying these techniques to a variety of impact conditions and intensities, necessary requirements have been developed to guide and evaluate the biofidelity of side impact ATD designs.

**NOMENCLATURE**

Symbol	Test Condition
RHF	Rigid high-speed flat wall
PHF	Padded high-speed flat wall
RLF	Rigid low-speed flat wall
PLF	Padded low-speed flat wall
RLT	Rigid low-speed thoracic offset
RLA	Rigid low-speed abdominal offset
RLP	Rigid low-speed pelvis offset
PLP	Padded low-speed pelvis offset

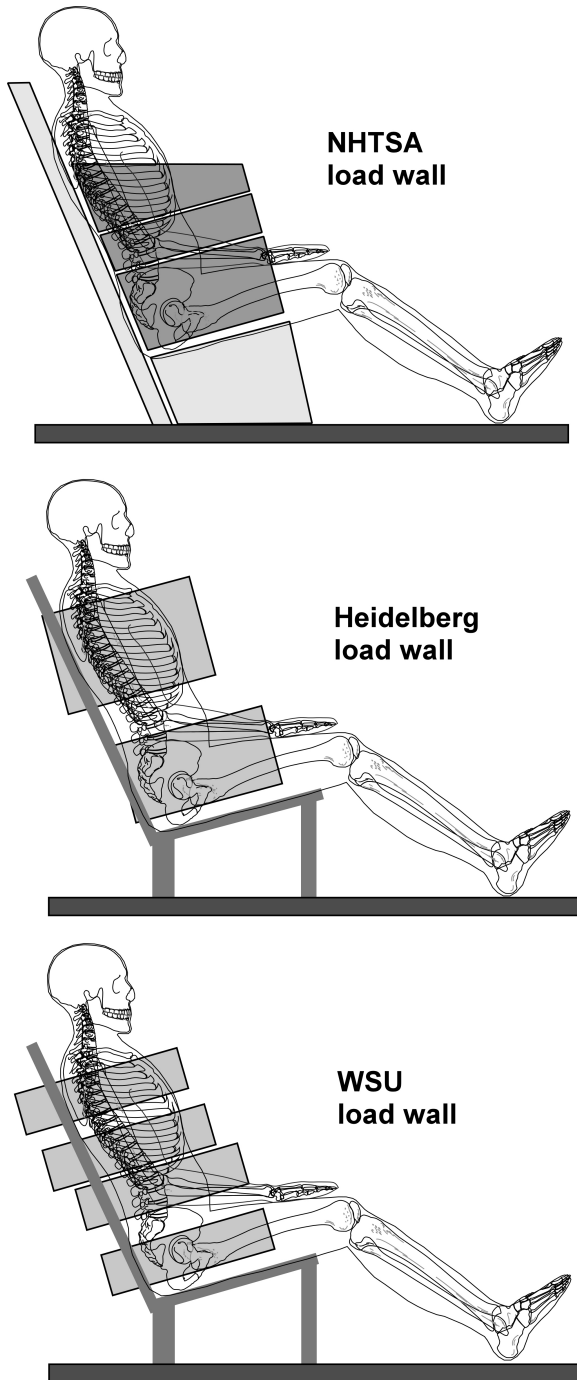


**Figure 6.** Comparison of load plate positions on the NHTSA, Heidelberg and Wayne State University (WSU) sleds, relative to the 50<sup>th</sup> percentile male.

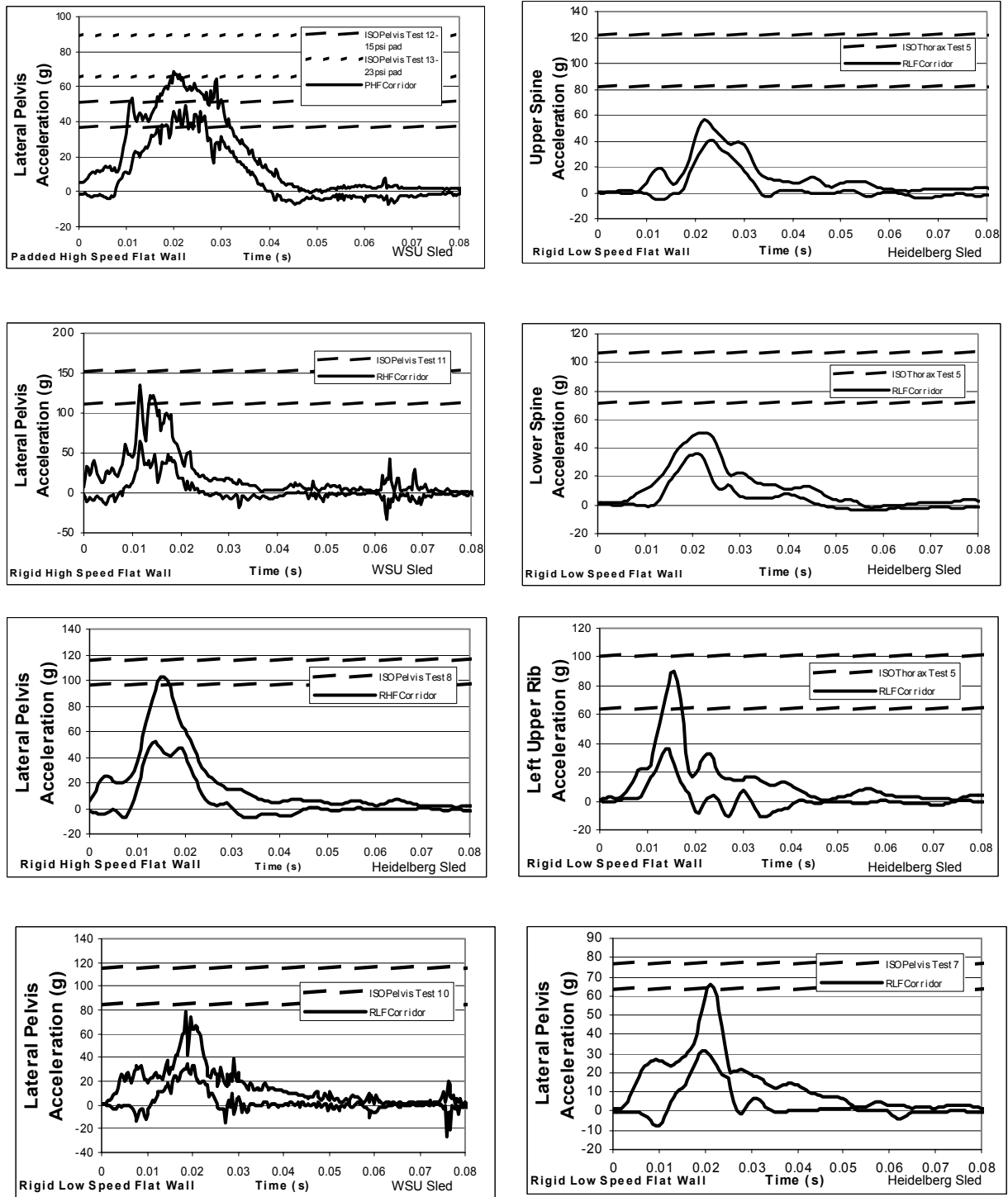
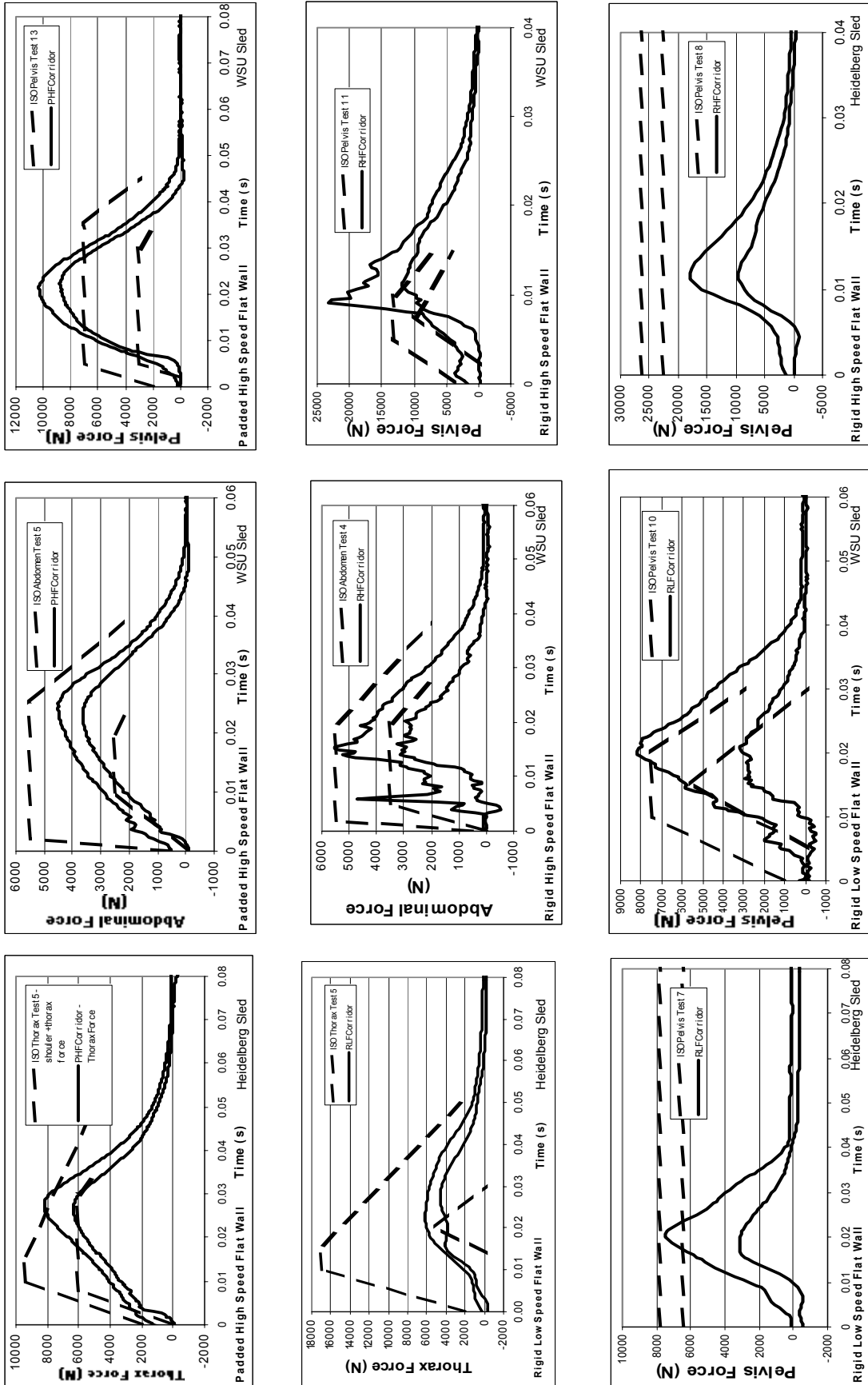


Figure 7. Rib, spine and pelvis accelerations – comparison with ISO TR9790 specifications for a side-impact dummy.



**Figure 8.** Thorax, abdomen and pelvis force – comparison with ISO TR9790 specifications for a side-impact dummy.

## REFERENCES

- Cavanaugh, J.M., Nyquist, G.W., Goldberg, S.J., and King, A.I. (1986) Lower abdominal tolerance and response, Proc. Thirtieth Stapp Car Crash Conference, pp. 41-63. Society of Automotive Engineers, Warrendale, PA.
- Cavanaugh, J.M., Zhu, Y., Huang, Y., and King, A.I. (1993) Injury and response of the thorax in side impact cadaveric tests. Proc. Thirty-Seventh Stapp Car Crash Conference, pp. 199-221. Society of Automotive Engineers, Warrendale, PA.
- Cavanaugh, J.M., Waliko, T., Chung, J., and King, A.I. (1996) Abdominal injury and response in side impact. Proc. Fortieth Stapp Car Crash Conference, pp. 1-16. Society of Automotive Engineers, Warrendale, PA.
- Eppinger, R.H. (1976) Prediction of thoracic injury using measurable experimental parameters. Proc. Sixth International Technical Conference on Experimental Safety Vehicles (ESV), pp. 770-780. United States Department of Transportation, Washington D.C.
- Eppinger, R.H. (1978) On the development of a deformation measurement system and its application toward developing mechanically based injury indices. Proc. Thirty-Third Stapp Car Crash Conference, pp. 21-28. Society of Automotive Engineers, Warrendale, PA.
- Eppinger, R.H., Marcus, J.H., and Morgan, R.M., (1984) Development of dummy and injury index for NHTSA's thoracic side impact protection research program. Proc. SAE Government/Industry Meeting, pp. 983-1011. Society of Automotive Engineers, Warrendale, PA.
- Eppinger, R.H. (2001) International harmonized research activities (IHRA) status report of the biomechanics working group. Proc. Seventeenth International Technical Conference on the Enhanced Safety of Vehicles (ESV) Conference. United States Department of Transportation, Washington, D.C.
- Irwin, A.L., Walilko, T.J., Cavanaugh, J.M., Zhu, Y., and King, A.I. (1993) Displacement responses of the shoulder and thorax in lateral sled impacts. Proc. Thirty-Seventh Stapp Car Crash Conference, pp. 165-174. Society of Automotive Engineers, Warrendale, PA.
- ISO/TR9790. (1999) Road vehicles-lateral impact response requirements to assess the biofidelity of the dummy. Technical Report No. 9790, International Standards Organization, American National Standards Institute, New York, NY.
- Kallieris, D., Mattern, R., Schmidt, G., and Eppinger, R.H. (1981) Quantification of side impact responses and injuries. Proc. Twenty-Fifth Stapp Car Crash Conference, pp. 329-368. Society of Automotive Engineers, Warrendale, PA.
- Krause, P.L. (1984) Normalization of side impact cadaver dynamic response data utilizing regression techniques. SAE Paper No. 840883, SAE Technical Paper Series, Government/Industry Meeting and Exposition. Society of Automotive Engineers, Warrendale, PA.
- Lobdell, T.E., Kroell, C.K., Schneider, D.C., and Hering, W.E. (1973) Impact response of the human thorax. in human impact response, pp. 201-245. Plenum Press, New York, NY.
- Mertz, H.J. (1984) A procedure for normalizing impact response data. SAE Paper No. 840884, SAE Technical Paper Series, Government/Industry Meeting and Exposition. Society of Automotive Engineers, Warrendale, PA.
- Morgan, R.M., Marcus, J.H., and Eppinger, R.H. (1981) Correlation of Side Impact Dummy/Cadaver Tests. Proc. Twenty-Fifth Stapp Car Crash Conference, pp. 301-326. Society of Automotive Engineers, Warrendale, PA.
- Morgan, R.M., Marcus, J.H., Eppinger, R.H., (1986) Side impact – the biofidelity of NHTSA's proposed ATD and efficacy of TTI. Proc. Thirtieth Stapp Car Crash Conference, pp. 27-40. Society of Automotive Engineers, Warrendale, PA.
- Pintar, F.A., Yoganandan, N., Hines, M.H., Maltese, M.R., McFadden, J., Saul, R., Eppinger, R., Khaewpong, N., and Kleinberger, M. (1997) Chestband analysis of human tolerance to side impact. Proc. Forty-First Stapp Car Crash Conference, pp. 63-89. Society of Automotive Engineers, Warrendale, PA.

Roberts, A. K., Janssen, E. G., and Cersari, D. (1990) Review of cadaver responses to lateral impact and derived biofidelity targets for dummies. Report of EEVC/WG9, IRCOBI Proceedings, Lyon, France.

Rouhana, S.W., and Kroell, C.K. (1989) The effect of door topography on abdominal injury in lateral impact. Proc. Thirty-Third Stapp Car Crash Conference, pp. 143-151. Society of Automotive Engineers, Warrendale, PA.

Viano, D.C. (1989) Biomechanical responses and injuries in blunt lateral impact. Proc. Thirty-Third Stapp Car Crash Conference, pp. 113-142. Society of Automotive Engineers, Warrendale, PA.

Zhu, J.Y., Cavanaugh, J.M., and King, A.I. (1993) Pelvic biomechanical response and padding benefits in side impact based on a cadaveric test series. Proc. Thirty-Seventh Stapp Car Crash Conference, pp. 223-233. Society of Automotive Engineers, Warrendale, PA.

APPENDIX A

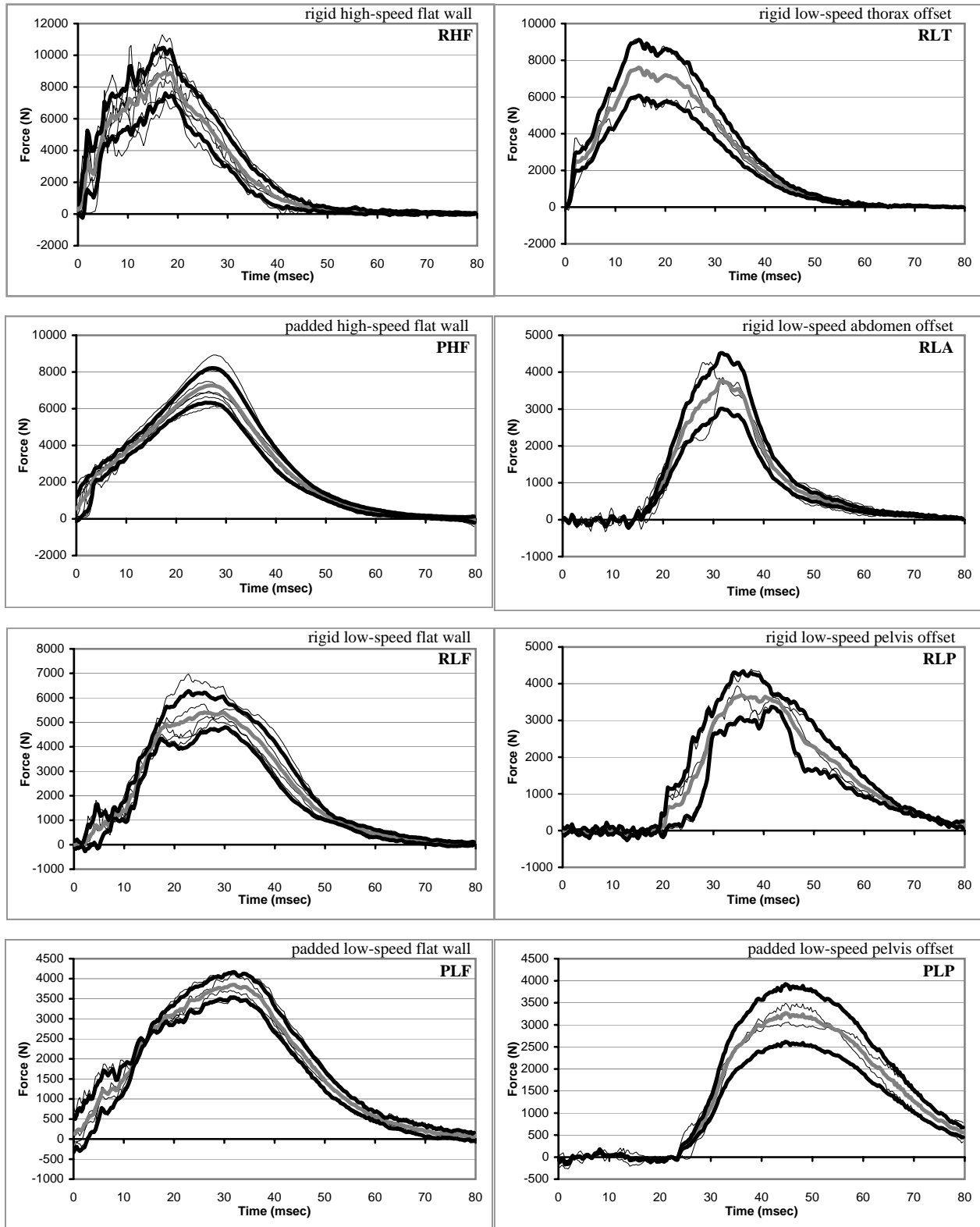


Figure A1. Thorax load wall force-time histories (CFC 1000). Individual PMHS runs are shown in thin lines; mean response is dark grey; corridor is dark black.

APPENDIX A

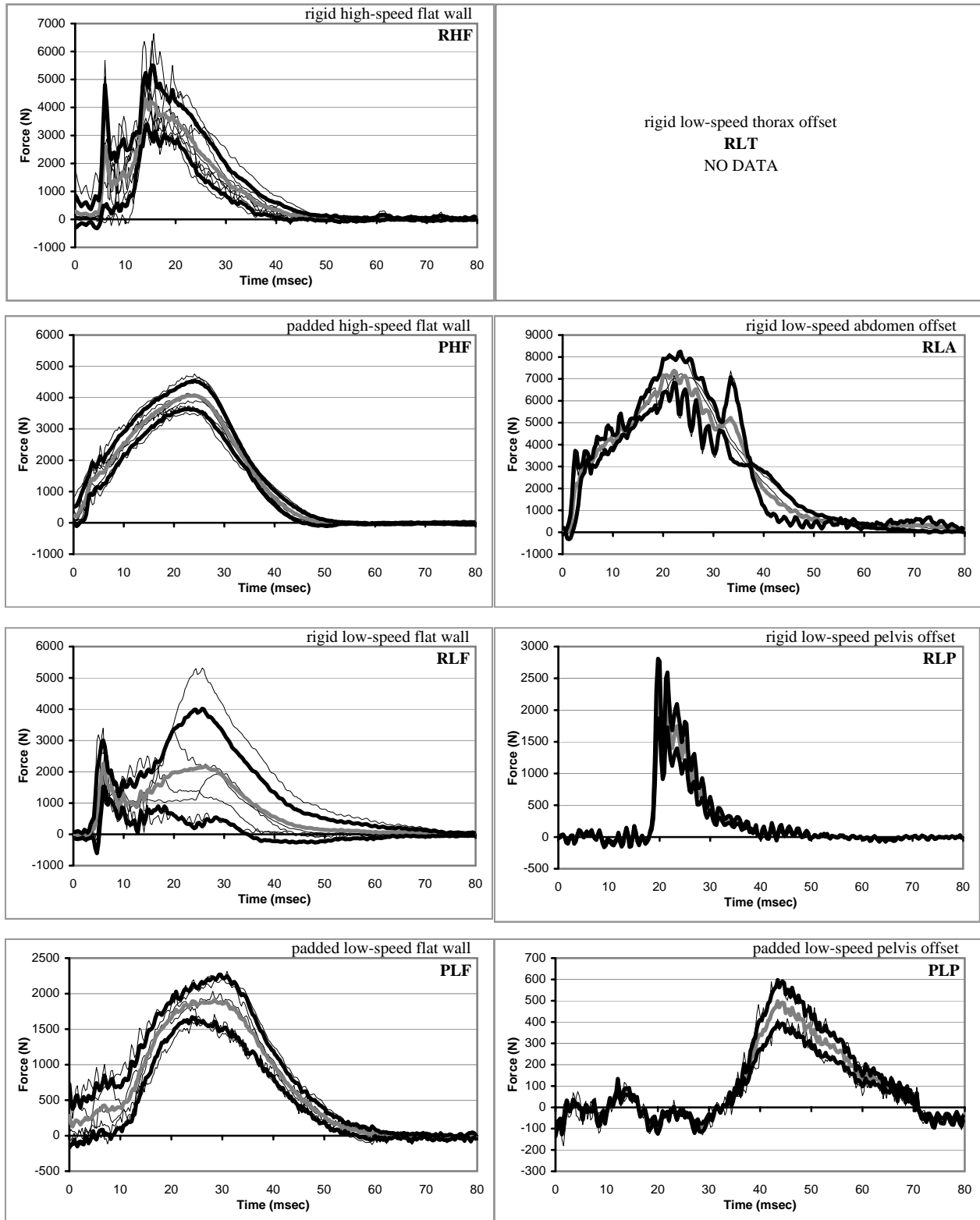


Figure A2. Abdomen load wall force-time histories (CFC 1000). Individual PMHS runs are shown in thin lines; mean response is dark grey; corridor is dark black.

APPENDIX A

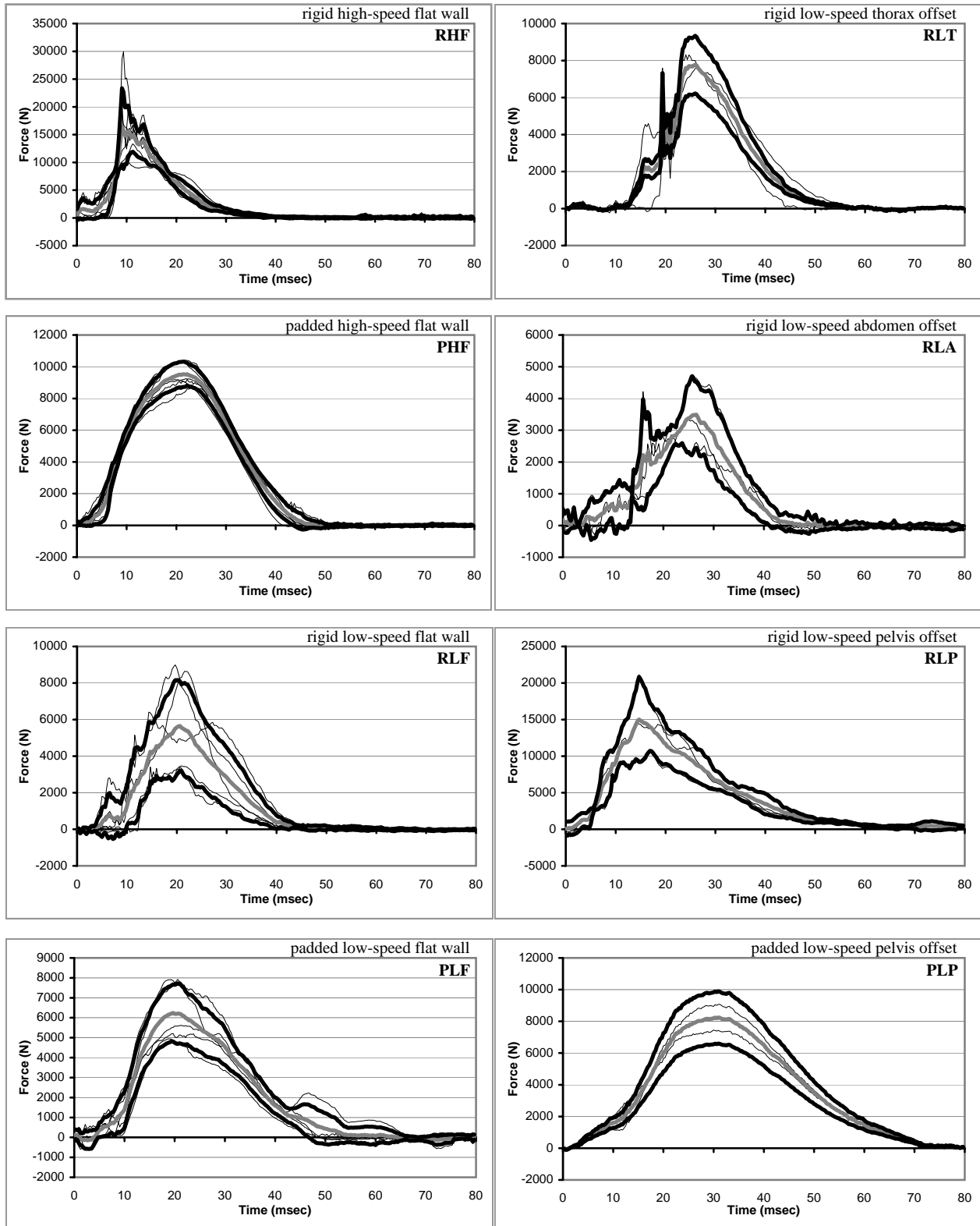


Figure A3. Pelvis load wall force-time histories (CFC 1000). Individual PMHS runs are shown in thin lines; mean response is dark grey; corridor is dark black.

APPENDIX A

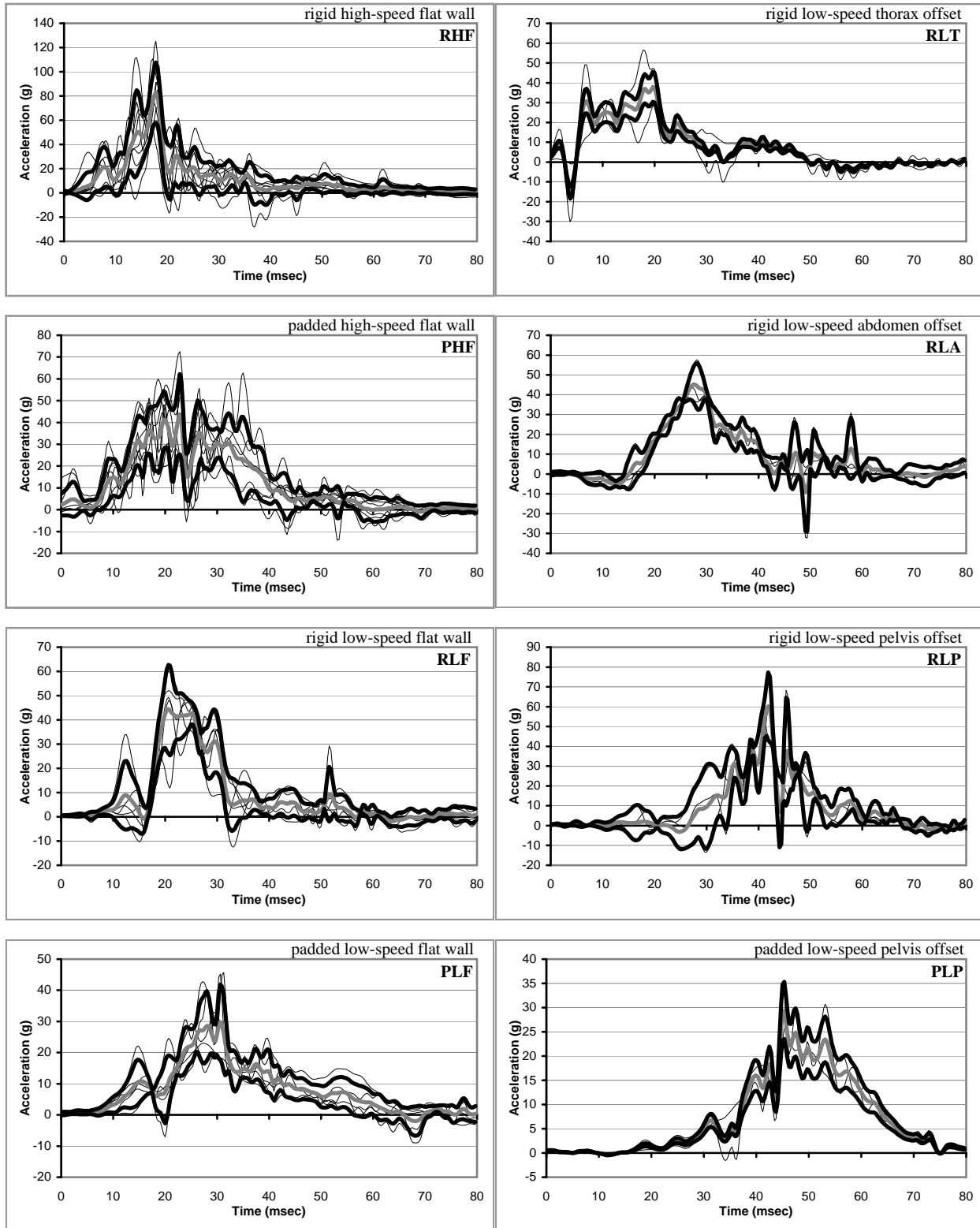


Figure A4. Upper spine lateral acceleration-time histories (CFC 180). Individual PMHS runs are shown in thin lines; mean response is dark grey; corridor is dark black.

APPENDIX A

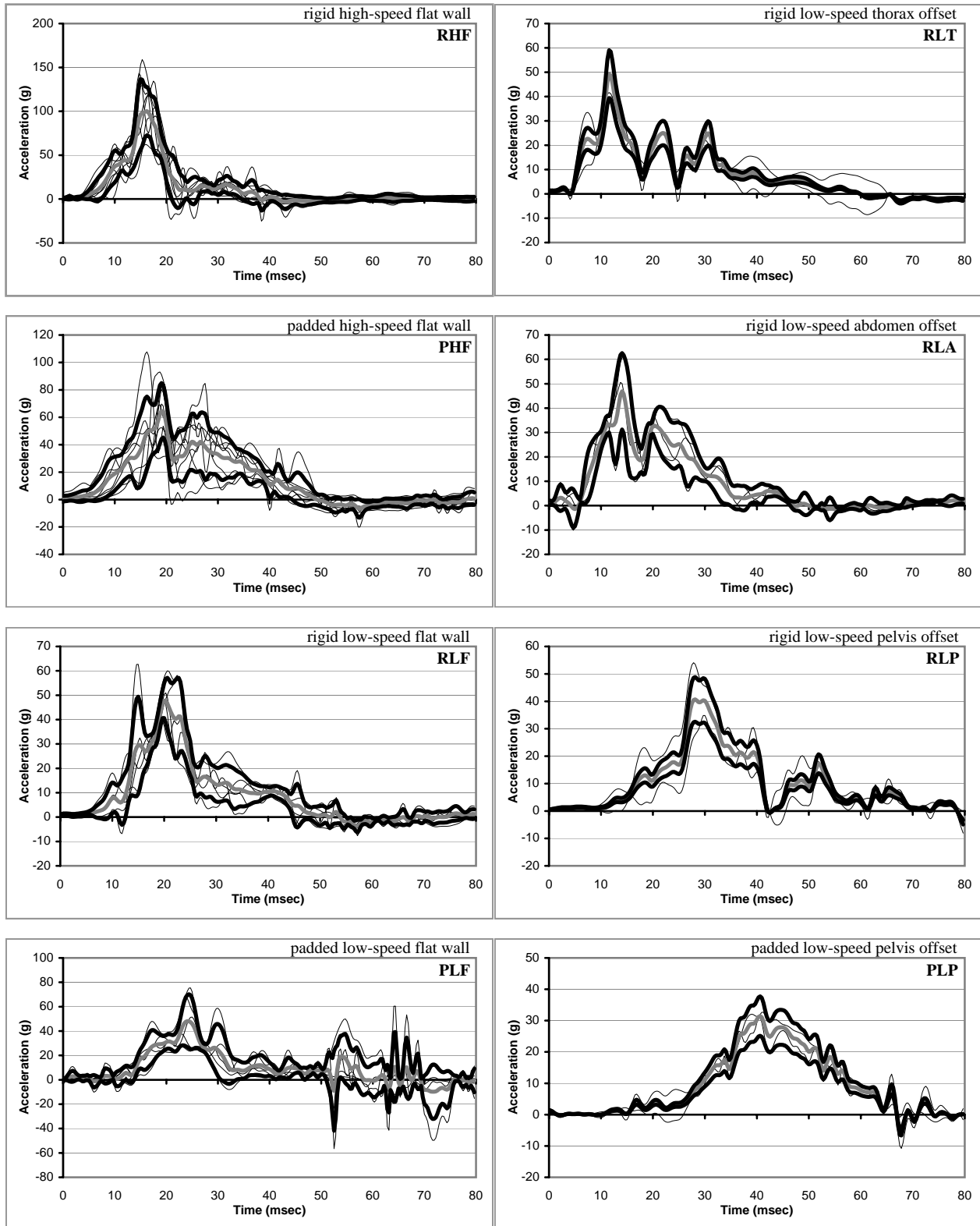


Figure A5. Lower spine lateral acceleration-time histories (CFC 180). Individual PMHS runs are shown in thin lines; mean response is dark grey; corridor is dark black.

APPENDIX A

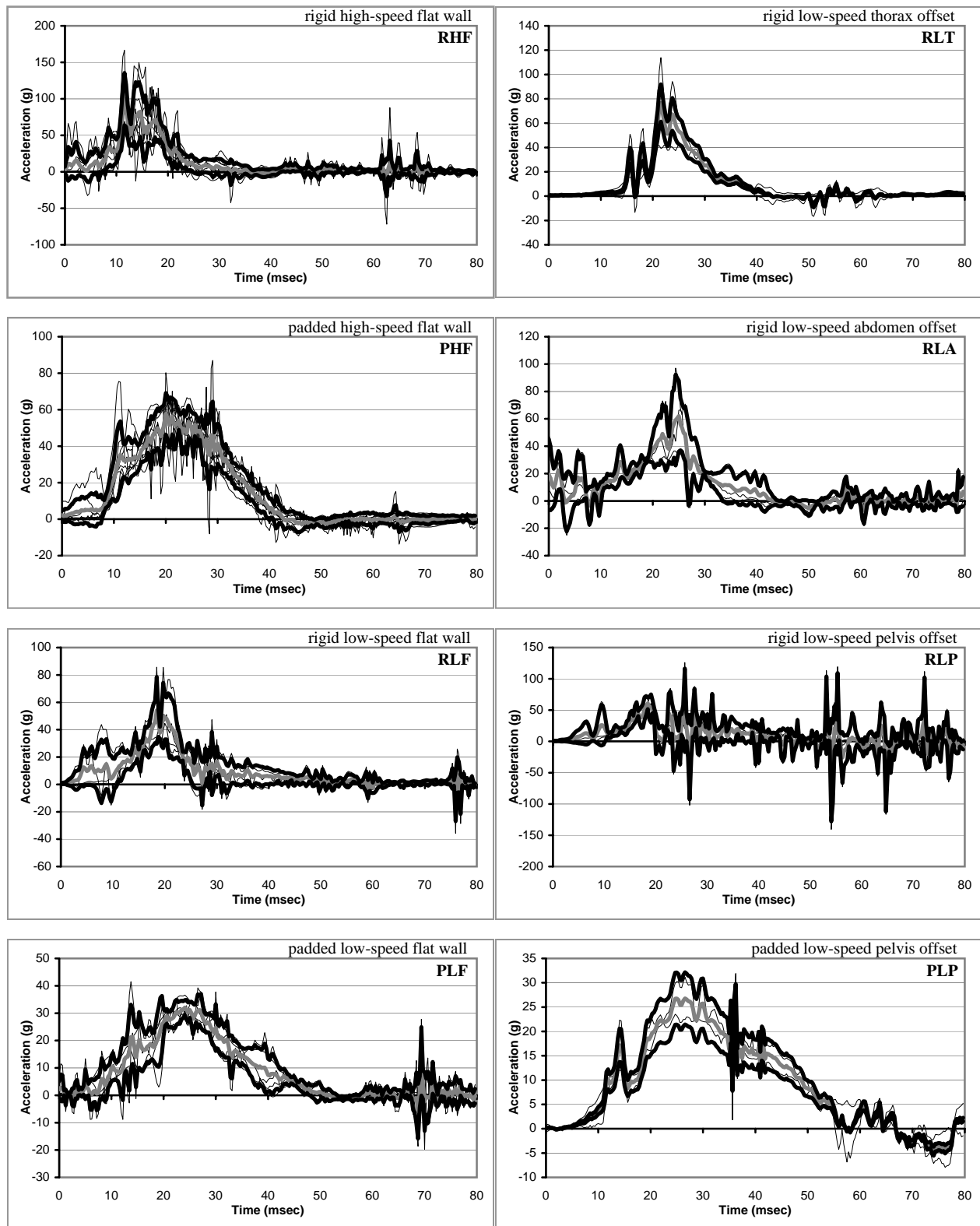


Figure A6. Pelvis lateral acceleration-time histories (CFC 1000). Individual PMHS runs are shown in thin lines; mean response is dark grey; corridor is dark black.

APPENDIX A

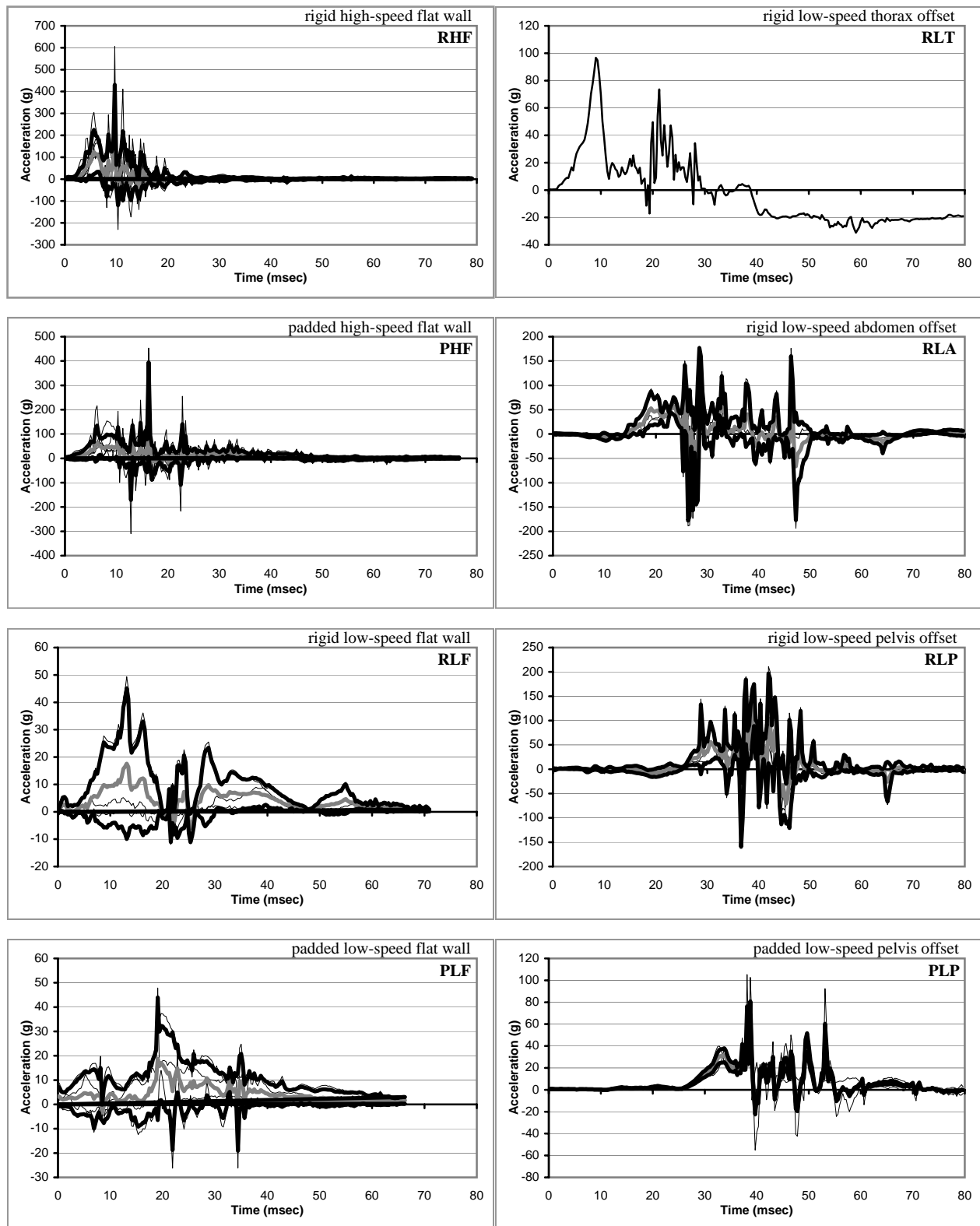


Figure A7a. Upper struck-side rib lateral acceleration-time histories (CFC 1000). Individual PMHS runs are shown in thin lines; mean response is dark grey; corridor is dark black.

APPENDIX A

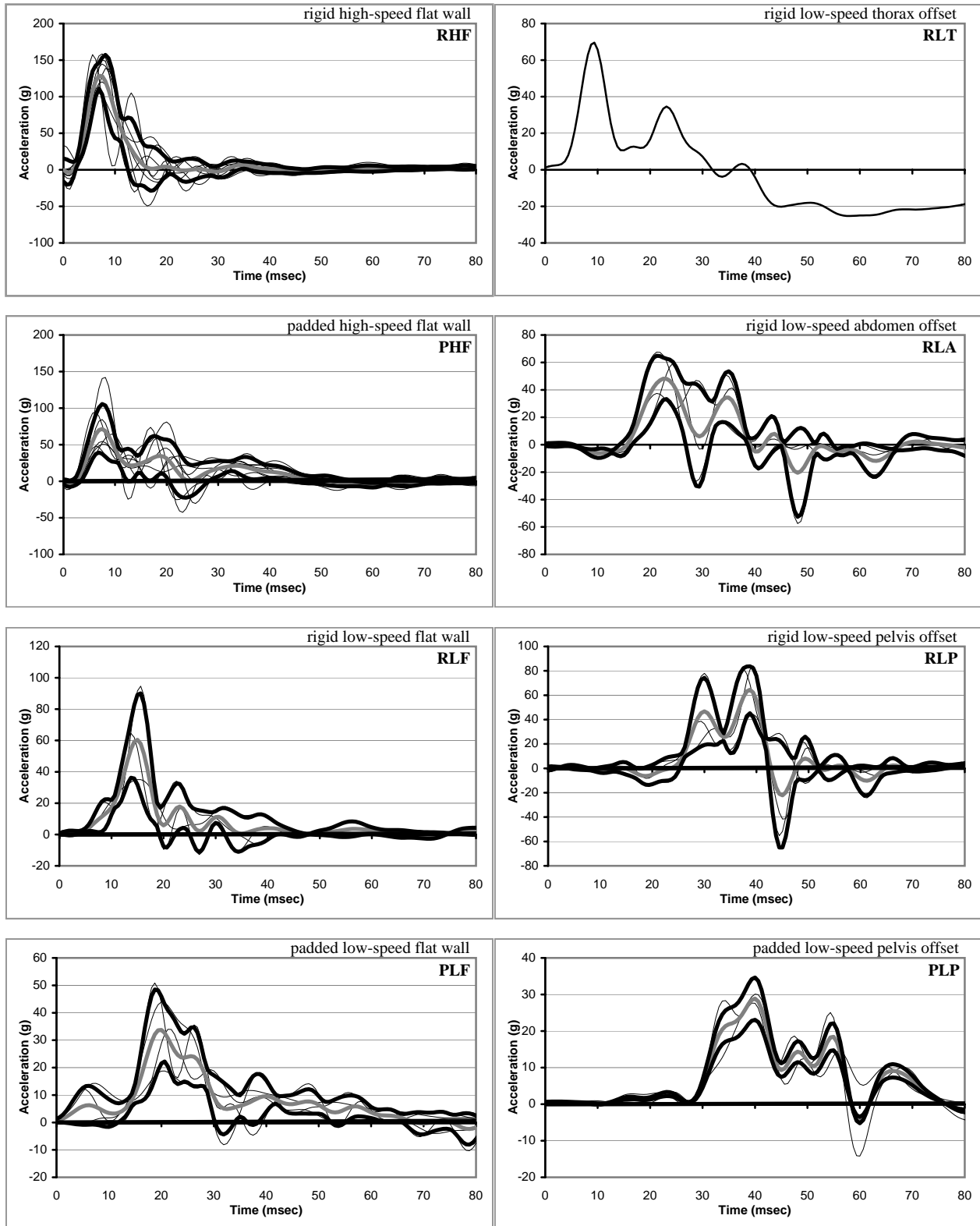


Figure A7b. Upper struck-side rib lateral acceleration-time histories (FIR 100). Individual PMHS runs are shown in thin lines; mean response is dark grey; corridor is dark black.

APPENDIX A

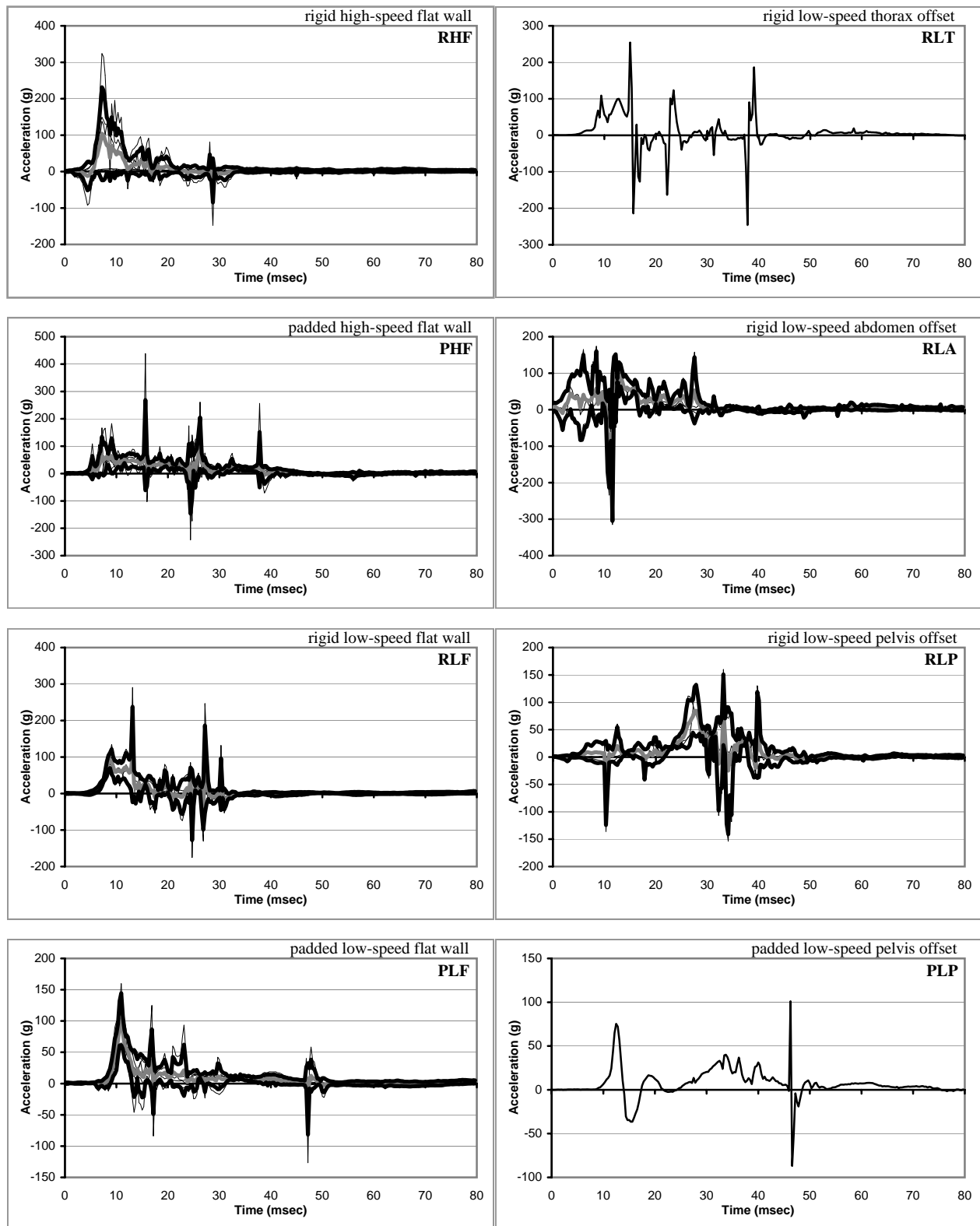


Figure A8a. Lower struck-side rib lateral acceleration-time histories (CFC 1000). Individual PMHS runs are shown in thin lines; mean response is dark grey; corridor is dark black.

APPENDIX A

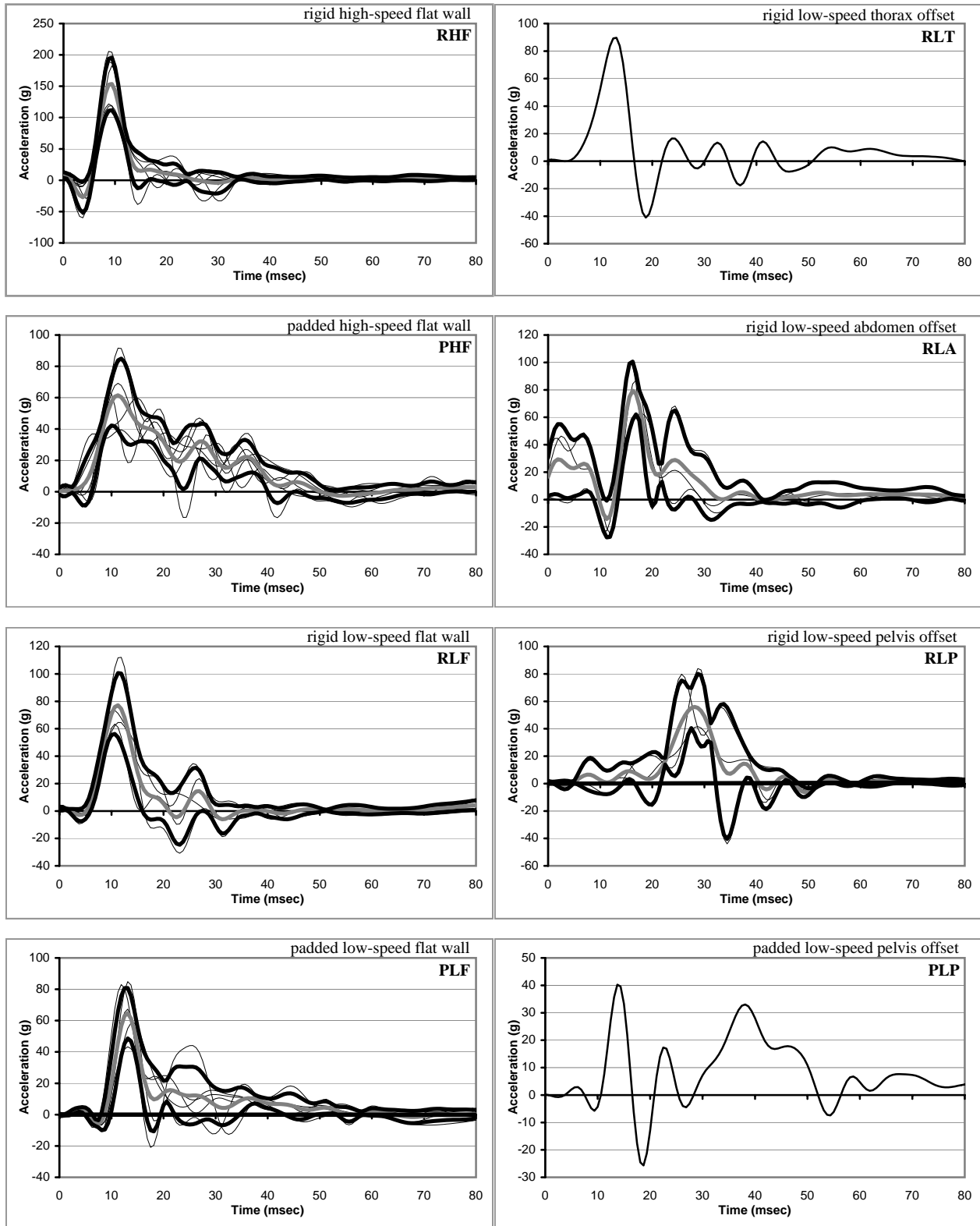


Figure A8b. Lower struck-side rib lateral acceleration-time histories (FIR 100). Individual PMHS runs are shown in thin lines; mean response is dark grey; corridor is dark black.

APPENDIX A

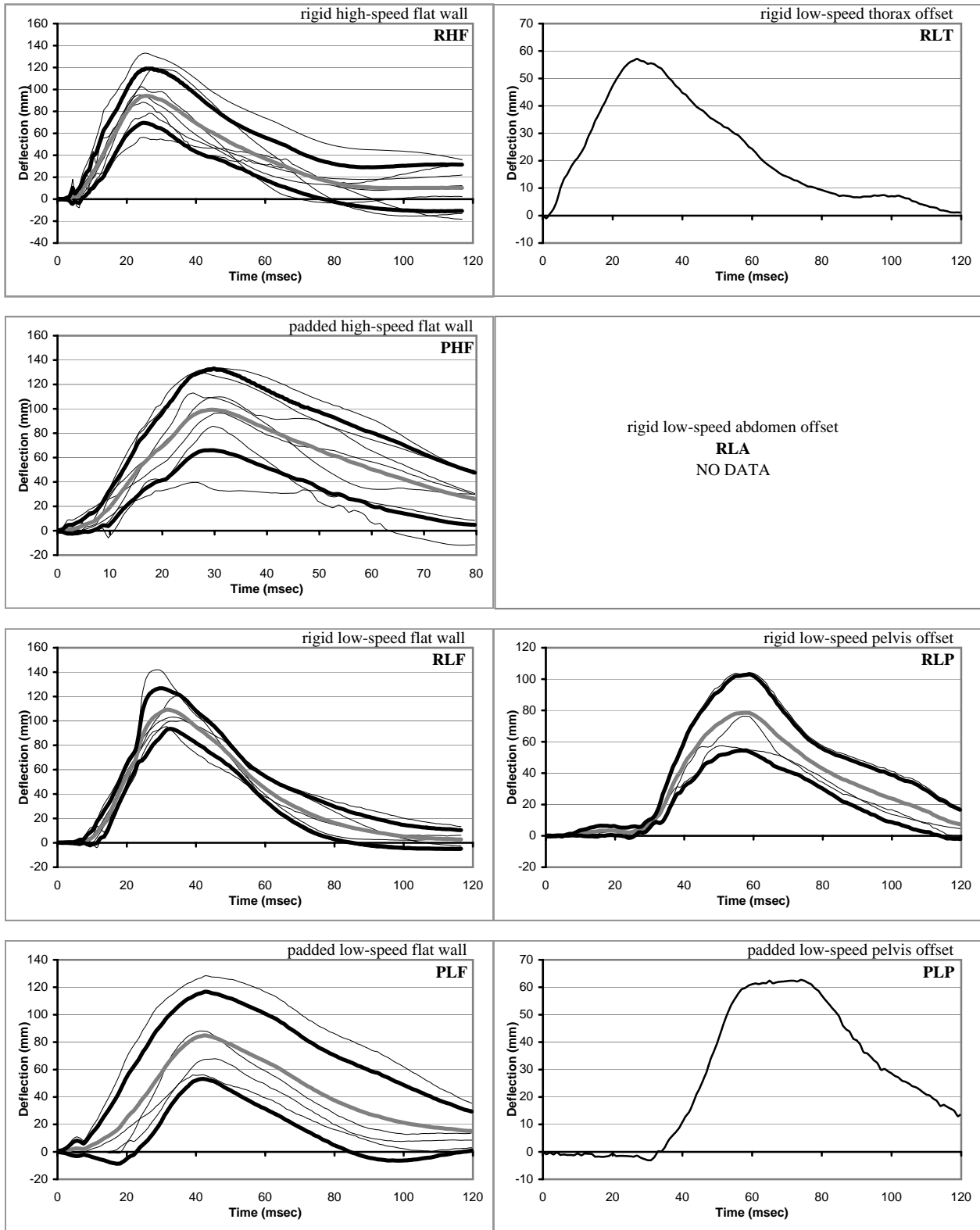


Figure A9. Upper thorax full-deflection-time histories (CFC 600). Individual PMHS runs are shown in thin lines; mean response is dark grey; corridor is dark black.

APPENDIX A

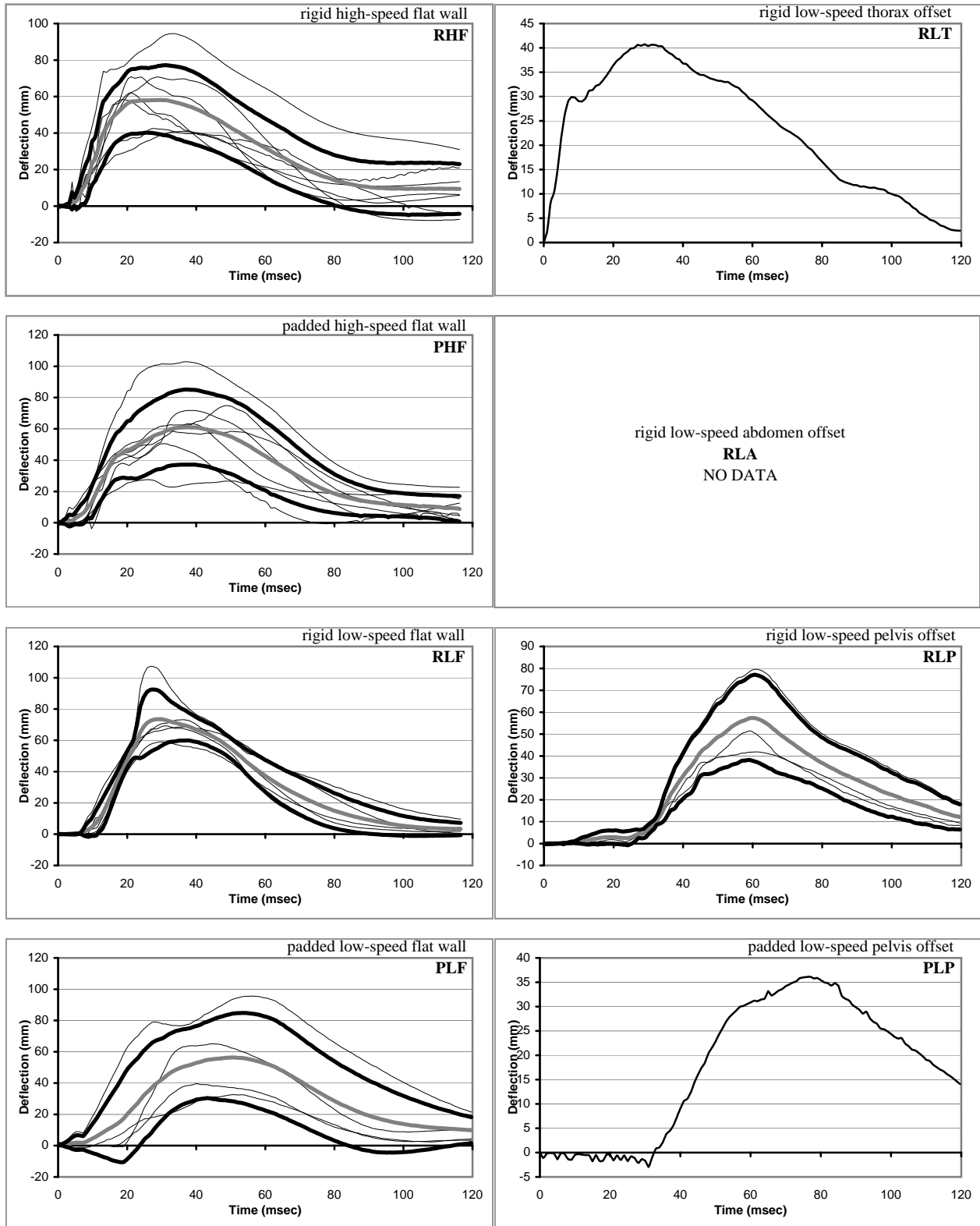


Figure A10. Upper thorax half-deflection-time histories (CFC 600). Individual PMHS runs are shown in thin lines; mean response is dark grey; corridor is dark black.

APPENDIX A

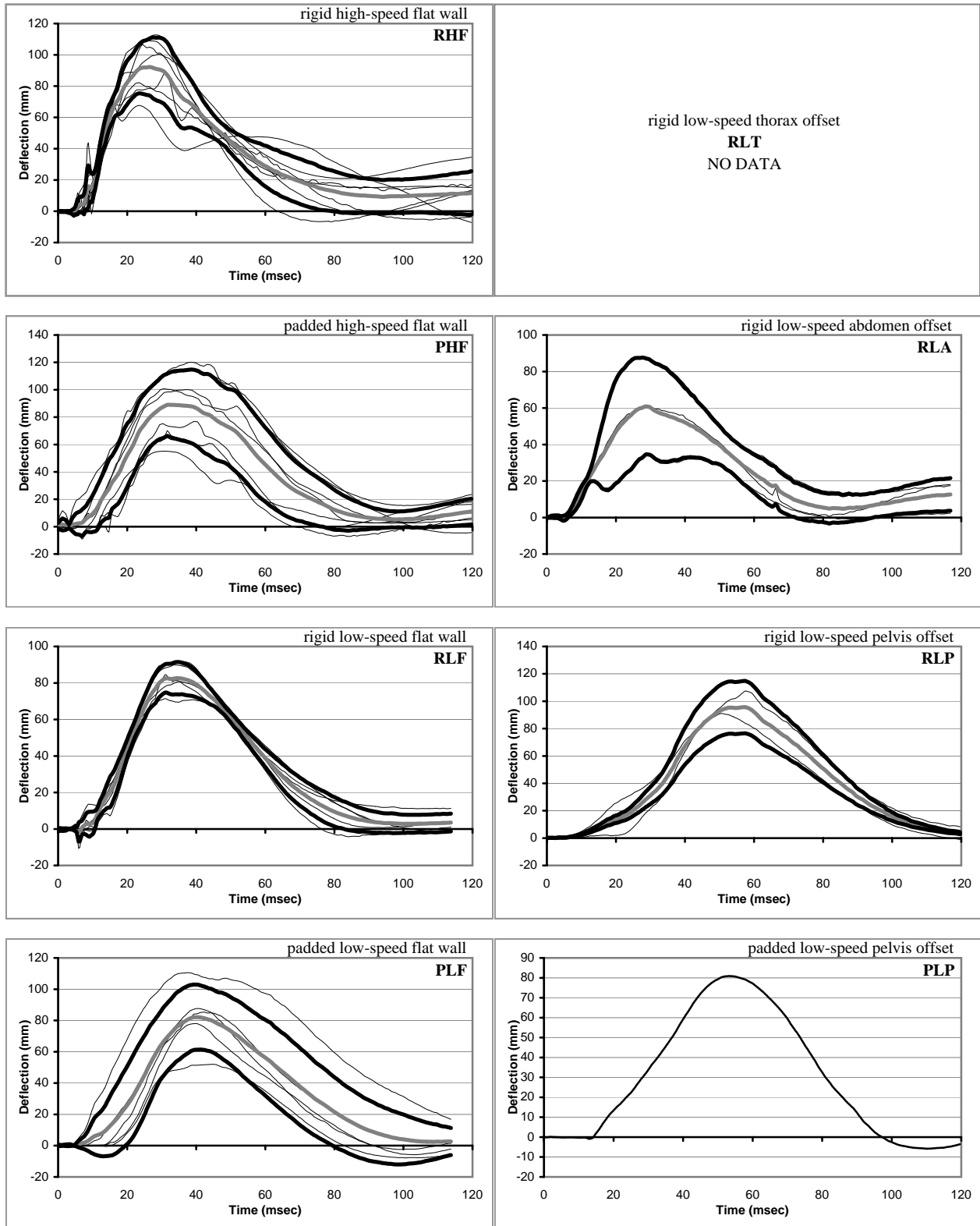


Figure A11. Lower thorax full-deflection-time histories (CFC 600). Individual PMHS runs are shown in thin lines; mean response is dark grey; corridor is dark black.

APPENDIX A

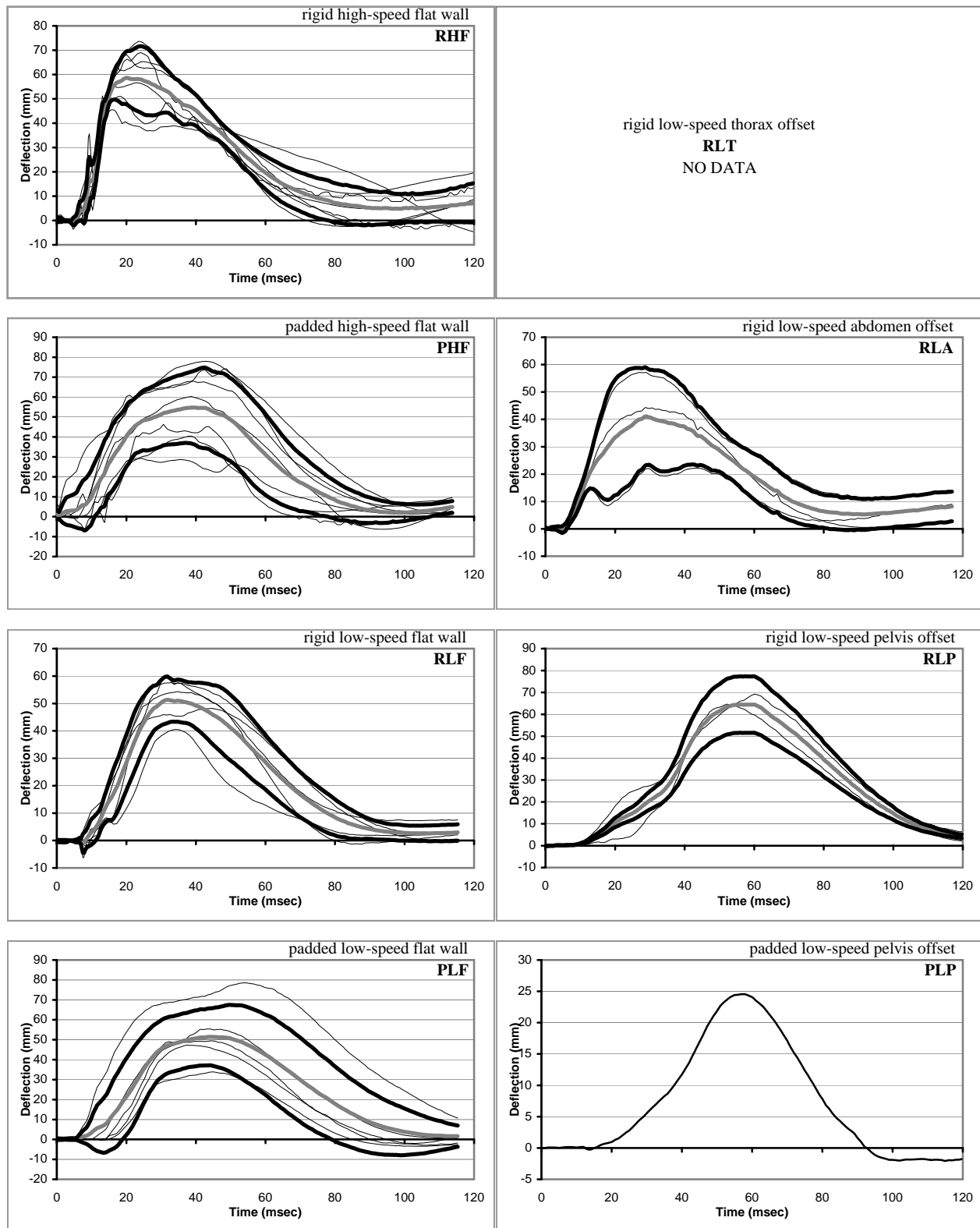


Figure A12. Lower thorax half-deflection-time histories (CFC 600). Individual PMHS runs are shown in thin lines; mean response is dark grey; corridor is dark black.

APPENDIX A

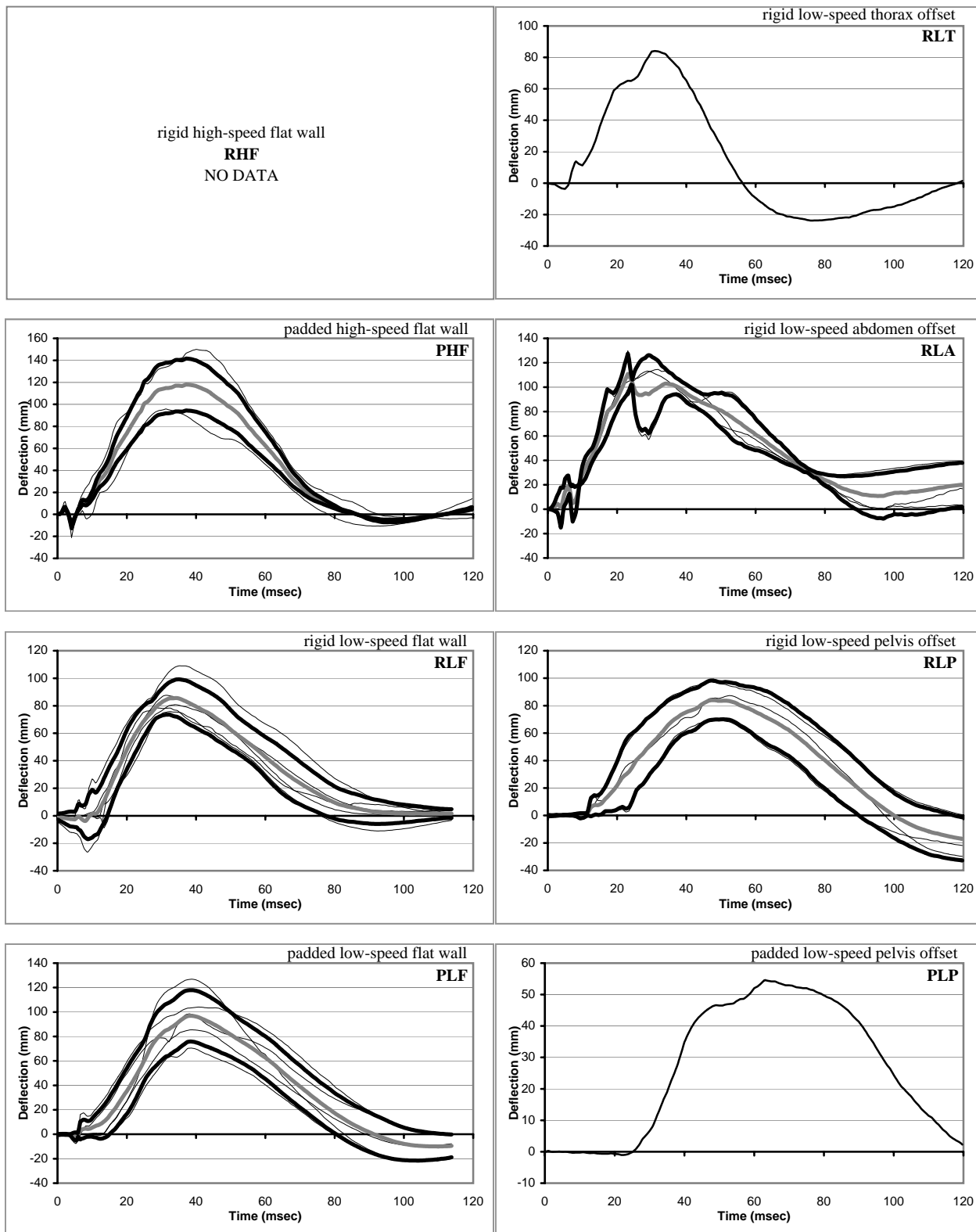


Figure A13. Abdomen full-deflection-time histories (CFC 600). Individual PMHS runs are shown in thin lines; mean response is dark grey; corridor is dark black.

APPENDIX A

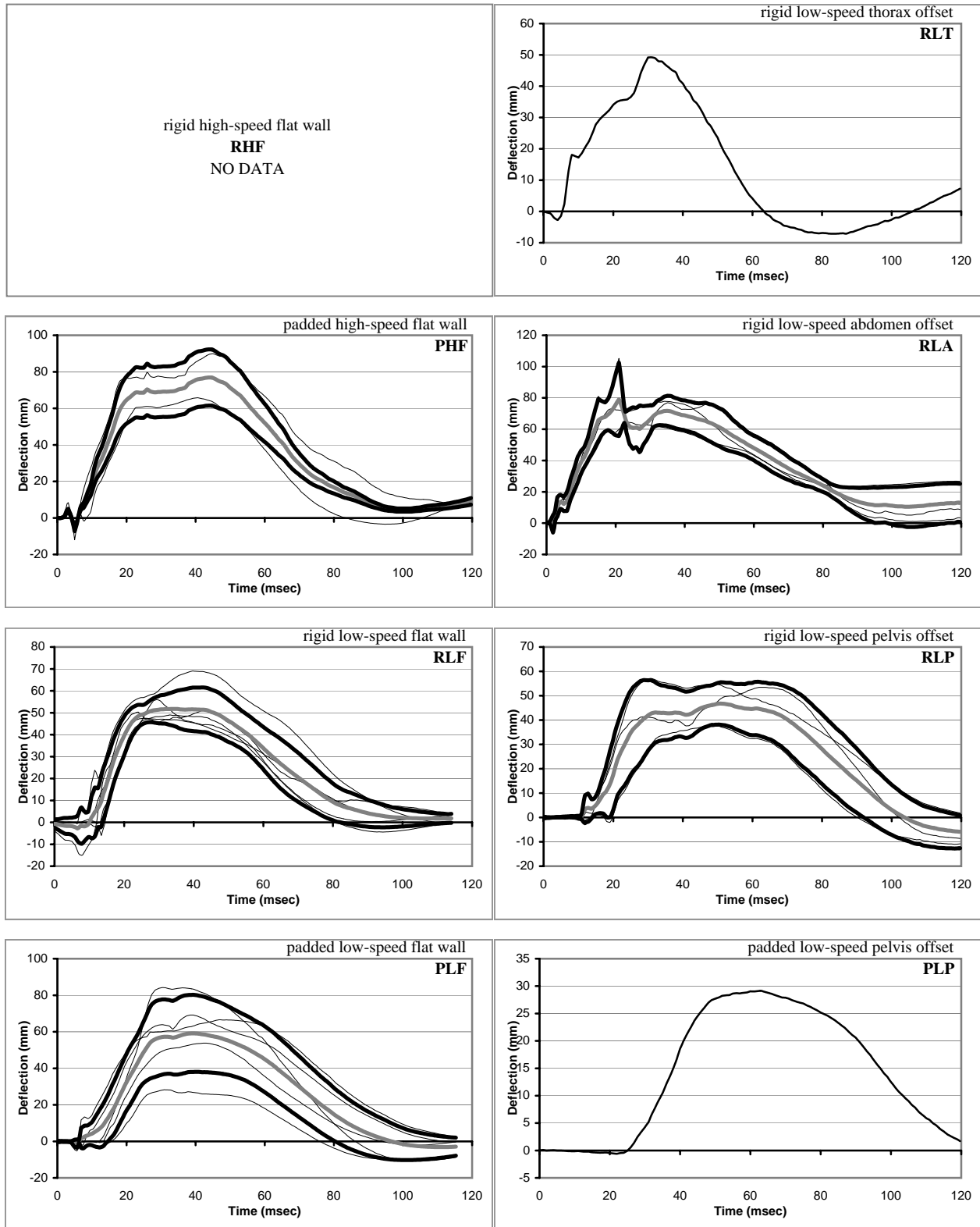


Figure A14. Abdomen half-deflection-time histories (CFC 600). Individual PMHS runs are shown in thin lines; mean response is dark grey; corridor is dark black.

APPENDIX B

Table B1. Test subject characteristics, injury, and maximum scaled load wall forces, accelerations, and deflections.

Test #	Test Type	Mass (kg)	Sex	Age (yrs)	# Rib Fx	# Fx Ribs	Load Wall Forces (N)			Acceleration (g)				Deflections (mm)							
							CFC 1000			Spine		Left Side Ribs		CFC 1000		Upper Thorax		Lower Thorax		Abdomen	
							Thorax	Abdomen	Pelvis	Upper	Lower	FIR 100	Upper	Lower	CFC 1000	Full	Half	Full	Half	Full	Half
3320	PHF	74	F	82	0	0	6152	3740	9206	55	70	84	60	64	134	115	103	78	73	51	
3321	PHF	42	F	75	13	13	6658	4136	9245	51	108	142	85	80	113	77	63	40	62	94	
3323	PHF	81	F	59	22	22	8927	4622	9189	57	85	64	69	68	130	100	72	60	63	69	
3580	PHF	56	M	75	19	19	6869	4088	10407	44	69	54	47	75	40	55	28	29	48	61	
3581	PHF	45	F	80	10	10	6955	4759	10342	50	80	95	---	64	86	70	51	46	61	65	
3586	PHF	67	M	79	9	9	8078	3904	10333	57	60	48	92	63	---	---	---	---	59	50	
3276	PLF	71	M	70	14	14	3497	2028	5619	23	68	34	59	34	---	52	---	34	24	58	
3277	PLF	64	M	56	0	0	---	1708	4942	23	75	19	43	37	68	85	33	55	23	63	
3719	PLF	53	M	79	2	2	4139	2032	7908	33	38	51	85	42	56	78	40	47	34	35	
3661	PLP	51	M	74	1	1	3491	416	9071	26	31	30	40	32	---	81	---	25	27	28	
3662	PLP	73	M	59	4	4	3060	600	7448	35	75	28	---	31	63	---	36	---	36	33	
3324	RHF	75	M	77	3	3	9950	6639	20056	91	134	120	---	100	133	88	95	51	105	120	
3325	RHF	61	M	63	22	22	8895	4271	16765	59	129	145	---	102	78	70	42	57	91	107	
3422	RHF	83	M	44	16	16	---	3846	9898	93	62	---	---	88	119	100	71	68	94	59	
3423	RHF	62	M	49	3	3	7241	3683	19397	112	75	139	111	70	103	113	71	74	117	58	
3577	RHF	52	F	74	5	5	7769	4785	13343	125	95	158	206	86	88	109	58	65	121	91	
3578	RHF	51	F	73	24	24	9442	6379	29920	72	143	105	183	167	95	106	62	69	74	117	
3579	RHF	98	M	68	16	16	11294	5146	20781	76	159	150	189	150	56	82	41	46	89	136	
3585	RHF	73	M	72	8	8	10719	5507	---	111	119	159	122	145	---	---	---	---	118	96	
3587	RHF	100	M	63	17	17	---	---	---	63	85	---	---	64	96	120	59	74	73	63	
3589	RHF	76	M	67	12	12	7484	3524	8683	72	93	50	64	87	110	101	75	68	73	86	
4218	RLA	81	M	68	7	7	4272	8171	4753	39	41	47	63	45	---	35	---	22	67	40	
4268	RLA	90	M	54	7	7	3857	7234	3346	44	61	68	100	97	---	61	---	44	52	52	
4295	RLA	52	F	51	5	5	---	7361	2855	58	51	59	87	66	---	88	---	57	60	45	
3120	RLF	89	M	73	6	6	5548	1925	3468	49	47	---	112	---	142	71	107	48	50	39	
3122	RLF	72	M	27	7	7	6968	2840	8641	60	58	35	---	86	100	85	69	60	62	54	
3155	RLF	76	M	55	0	0	4991	5314	3408	49	51	95	65	61	121	81	73	58	50	43	
3588	RLF	66	M	72	7	7	4161	2312	5211	46	29	44	67	37	128	111	96	79	49	26	
3663	RLF	42	F	75	8	8	3711	2200	7923	45	51	---	83	39	88	88	65	49	47	45	
3664	RLF	74	F	67	8	8	5263	3385	6407	52	63	65	73	44	95	92	59	41	54	60	
3700	RLF	67	M	86	0	0	5743	3392	8988	47	41	---	63	51	103	90	69	54	47	39	
3535	RLP	88	M	78	6	6	3656	---	10836	77	35	84	42	126	104	108	80	69	79	33	
3536	RLP	76	M	84	8	8	3944	---	14424	68	---	78	84	119	58	91	42	65	69	---	
3537	RLP	93	M	79	8	8	4400	2340	21127	55	54	82	80	112	76	---	52	---	57	50	
4296	RLT	66	M	39	10	10	6084	2037	8315	49	57	---	---	114	57	101	41	100	51	43	
4338	RLT	69	F	46	7	7	9159	129	7654	57	42	70	90	43	---	---	---	---	64	37	